UNIVERSITY OF CALIFORNIA,
IRVINE

Design and Methodology for Optimization of Polymer Sensing for Three Target Analytes

DISSERTATION

submitted in partial satisfaction of the requirements
for the degree of

DOCTOR OF PHILOSOPHY

in Chemistry

by

Crystin Jän Eggers

Dissertation Committee:
Professor Reginald M. Penner, Chair
Professor Robert M. Corn
Professor Sergey Nizkorodov

2017

DEDICATION

To
My nieces and nephew,
Aowyn, Pennie, Wyatt, and Genesee,
You are my light when all is dark.

TABLE OF CONTENTS

LIST OF FIGURES

LIST OF TABLES

Page

ACKNOWLEDGMENTS

I would like to thank Professor Reginald M. Penner for the opportunities and experience he provided as my adviser, for teaching me many things over the years, some I knew I would learn and many that I didn't expect. I have grown as a person and a scientist while working under his tutelage.

I would like to express appreciation to professor Robert M. Corn and professor Sergey Nizkorodov for treating me like a member of their own research groups. I greatly appreciate the encouragement and help they both provided me over the years. Both opened their doors to me when I was in need and treated me as a colleague. Rob taught me to be a better investigator, a patient teacher, and an effective communicator. Sergey adopted me into his lab and gave me a second home. He looked out for my best interests as well as my progress, encouraged me when I was down, celebrated with me when I was up, and provided a safe place for me to express concerns and ideas.

Permission to use copyrighted material for chapter 2 of this manuscript has been granted from the American Chemical Society. Permission to use copyrighted material for figures 3.1 and 3.2 in this manuscript has been granted by the Creative Commons Attribution 3.0 Unported License from the Royal Chemical Society of Chemistry and InTechOpen open access book publisher.

Thank you to all my lab mates over the years for providing a wonderful working environment, especially those that I had the privilege of working with throughout my time here; Lindsay Kindra, Dr. Rajen Dutta, Dr. Mya Le Thai, Dr. Xaowei Li, Dr. Girija Chandran, and Alana Ogata. Additionally, I would like to thank all the staff members in the Chemistry departments, and physical science store, and the LEXI facility.

I would like to thank my friends and family. To Kelly Brown and her family for encouraging me and supporting me before, during, and I am sure after my graduate career. My parents for their contributions and support. To my brother and sister in-law for always pushing me to be better, picking me up when I fall down, and always taking care of me. To my grandparents for the free meals, love, support, free laundry, hugs, encouragement, and spare parts. To Dian Romonosky for tackling this great adventure and many others with me; there are no words to express my gratitude for your support and friendship. To Erinn and Andrew Parnell, thank you for all your help, support, encouragements, long talks, and game nights.

Lastly, I would like to thank Matthew Alden for being the love of my life.

CURRICULUM VITAE

Crystin Jän Eggers

EDUCATION

Doctor of Philosophy in Analytical Chemistry **2017**
University of California, Irvine *Irvine, California*

Bachelor of Art in Chemistry **2011**
California State University, Sacramento *Sacramento, California*

Associate of Arts in Accounting **2005**
Sierra College *Rocklin, California*

RESEARCH EXPERIENCE

Graduate Research Assistant **2011–2017**
University of California, Irvine *Irvine, California*

Undergraduate Research Assistant **2008–2010**
California State University, Sacramento *Sacramento, California*

TEACHING AND PROFESSIONAL EXPERIENCE

Teaching Assistant **2011–2016**
University of California, Irvine *Irvine, California*
- General Chemistry 1A, 1B, and 1C
- Organic Chemistry Laboratory 51LA and 51LB
- Quantitative Analysis, Chemistry 151 (Head TA)
- Electrochemistry, Chemistry 248

Outreach Program Coordinator **2011–2013**
University of California, Irvine *Irvine, California*

SELECTED HONORS AND AWARDS

Undergraduate Award in Analytical Chemistry **2009**
California State University, Sacramento *Sacramento, California*

Howell-CSUPERB Scholar **2009**
Dorris A. Howell Foundation for Women's Health *California*

Summer Undergraduate Research Experience **2009**
California State University, Sacramento *Sacramento, California*

REFEREED JOURNAL PUBLICATIONS

Lithographically Patterned PEDOT Nanowires for the Detection of Iron (III) with Nanomolar Sensitivity **2015**
Analytical Chemistry

ABSTRACT OF THE DISSERTATION

Design and Methodology for Optimization of Polymer Sensing for Three Target Analytes

By

Crystin Jän Eggers

Doctor of Philosophy in Chemistry

University of California, Irvine, 2017

Professor Reginald M. Penner, Chair

This dissertation explores the development of polymer sensors for three different targets and ways to improve sensor design, sensitivity, and reliable recognition elements. All sensors comprise three layers: recognition, interface, and transducer. These elements can be compiled from many different techniques depending on the desired target analyte and signal output. This research focuses on electrochemical impedance as the signal output, polymer films and nanowires as the interface, while varying the recognition layer and target analytes.

Chapter 1 reviews two different polymer types that incorporate specifically tailored filamentous bacteriophage virus M13 (phage), and the various architectures developed in attempt to optimize sensitivity, cost, and ease of fabrication. In chapter 2 arrays of nanowires of an electronically conductive polymeric affinity medium tailored to the detection of Fe(III) are prepared and their properties for detecting Fe(III) are evaluated. Lastly, chapter 3 explores the steps made towards making a non-enzymatic impedance based glucose sensor.

Chapter 1

Protein Detection

1.1 Abstract

The goal of this research is to make an ultra-cheap, disposable urine assay that specifically binds and measures various protein bio-markers for the purpose of early cancer detection. This chapter reviews two different polymer types that incorporate specifically tailored filamentous bacteriophage virus M13 (phage), and the various architectures developed in attempt to optimize sensitivity, cost, and ease of fabrication. The sensor is constructed in two ways, either by electrodeposition of poly(3,4-ethylenedioxythiophene), PEDOT, or by drop casting polyethyleneimine (PEI), both in the presence of phage. The resulting polymer-phage surfaces maintain their ability to recognize and bind proteins of interest as well as having limited non-specific binding. Electrochemical impedance spectroscopy (EIS) is used to detect the changes in impedance before and after exposure to a target analyte solution. Scanning electron microscopy (SEM), atomic force microscopy (AFM), x-ray photoelectron spectroscopy (XPS), and fluorescent imaging are used to verify phage incorporation into the films.

1.2 Introduction

There is a great need and desire for point of care (POC) biosensors that are inexpensive, fast, reproducible, have non-invasive sample collection techniques, multi-analyte detection capabilities, and minimal sample processing. This chapter explores two polymer-phage sensors that attempt to address these needs by providing simple fabrication steps, independence from costly and unstable elements, new architectures, one step small volume sensing, and multi-channel sensor arrays.

All biosensors are comprised of three elements, the biological recognition layer (BRL), the transducer, and the interface, as shown in Figure 1.1. There are several different types of BRLs, the most popular being antibodies (ABs). Other types include DNA, enzymes, nucleic acids, and bacteriophage [12]. The first element is the BRL, which is responsible for interacting with the analyte by bonding [12]. As mentioned, ABs are the most common BRL due to highly specific affinities to analytes. However, ABs are expensive to manufacture, time-consuming (taking between 2–12 months), and require the harvesting of animal blood serum [39]. The second element is the transducer, which is responsible for transmitting a measurable signal that occurs when the BRL interacts with the target analyte. There are several types of transducers, some examples are electrochemical, optical, thermal, acoustic, and piezoelectric [12]. In this project electrochemical impedance spectroscopy is used, as described by Donovan and Mohan et al. [18, 35]. The interface is the third element and it combines the BRL and the transducer. This element must be compatible with both the BRL and transducer as well as have limited interaction with the target analyte or other substances in the sample solution.

To address these needs, without using ABs, the Penner and Weiss labs developed a protein sensor using a specifically tailored filamentous bacteriophage virus M13 (phage) as the BRL, and poly (3,4-ethylenedioxythiophene) (PEDOT) as the interface. Phage, shown in Figure

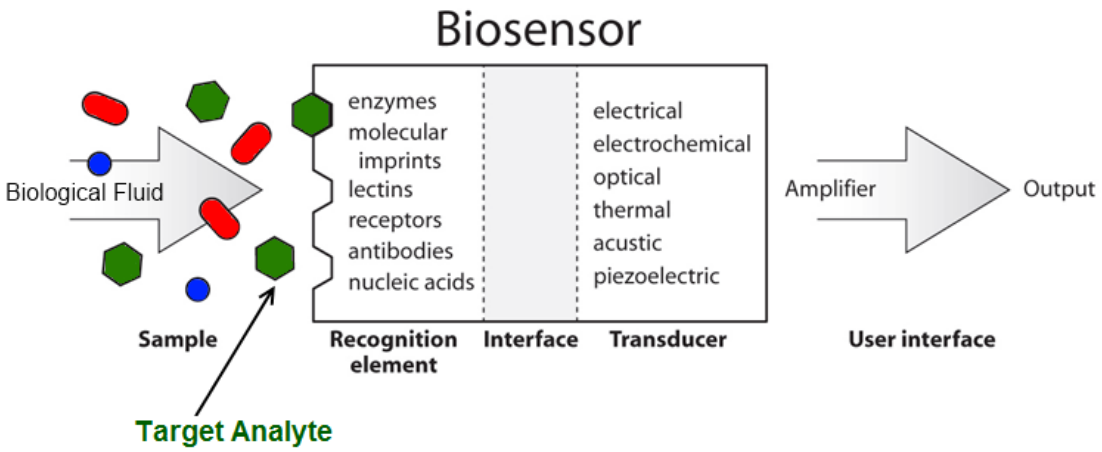

Figure 1.1: Elements of a biosensor, Figure by Chamber et al. [12]

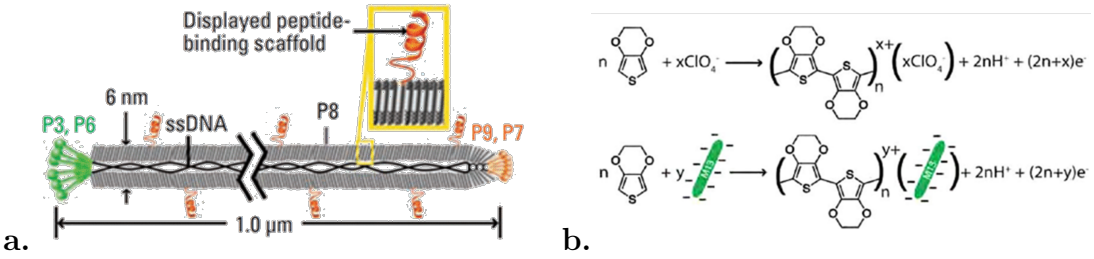

Figure 1.2: a. M13 bacteriophage (phage), b. Polymerization of EDOT and EDOT phage [7], the incorporation of phage into PEDOT is electrochemically polymerize at around 0.8–1.1 V versus SCE if a negative anion is present.

1.2a, is a virus that is easy to manufacture, inexpensive, can be made in large quantities, and can be modified to have an affinity for almost any specific analyte [39]. Phage are negatively charged on the surface, at the outer end of the P8 proteins.

PEDOT is a semi conducting polymer that polymerizes in the presence of negative molecules, as shown in 1.2b [18, 35, 39, 7, 61, 6, 17]. PEDOT has been shown to be non-reactive with target analytes, as well as capable of incorporating phage without hindering phage-protein binding properties [18, 35].

Previous works by the Penner lab [18, 35, 61, 6, 17] use a three electrode cell where the counter electrode (CE) was a platinum plate, the reference electrode (RE) was a silver/ silver chloride electrode (Ag-AgCl) or a saturated calomel electrode (SCE), and the working electrode (WE) was a 3 mm diameter gold electrode coated with an PEDOT-phage film, as shown in Figure 1.3a. These PEDOT-phage film biosensors require a CE which is costly and a RE which have potential for inaccurate measurements due to solution salt concentration and pH. One possible way to avoid this is to wash the sensor after exposure [35], but this adds extra processing steps. These sensors also require large solution volumes for electropolymerization and sensing, both Donovan and Mohan [18, 35] used 50 ml of plating and sensing solution, causing large volumes of phage and target analyte, respectively, to go to waste. New ways were explored to incorporate phage into a film using polyethyleneimine (PEI) and layer-by-layer (LBL) deposition.

PEI is a polymer with terminal amine groups that can have a positive charge at the correct pH. The use of layer-by-layer deposition exploits electrostatic force attraction, allowing absorption of alternating polyanions and polycations. PEI-phage films have been created by Yoo et al. [62], and they show how phage can be ordered into networks. These same fabrication steps are modified to create PEI-phage sensors.

PEDOT-phage – First, this chapter will discuss how devices from previous research using PEDOT-phage were modified to eliminate unnecessary elements, specifically the RE and CE, by reconstructing the electrode architecture using a two electrode system, shown in Figure 1.3b. The current limit of detection (LOD) for PEDOT-phage film based sensors is 100 pM for prostate specific membrane antigen (PSMA) [35]. Monitoring of prostate cancer patients urine PSMA values have shown an increase from 0.25 nM to 3.5 nM, making the current biosensor a good method for monitoring PSMA levels [9]. However, as discussed above, the design of this sensor leaves much to be desired. Along with architecture changes a new phage was used, due to the unavailability of the target analyte PSMA, and therefore

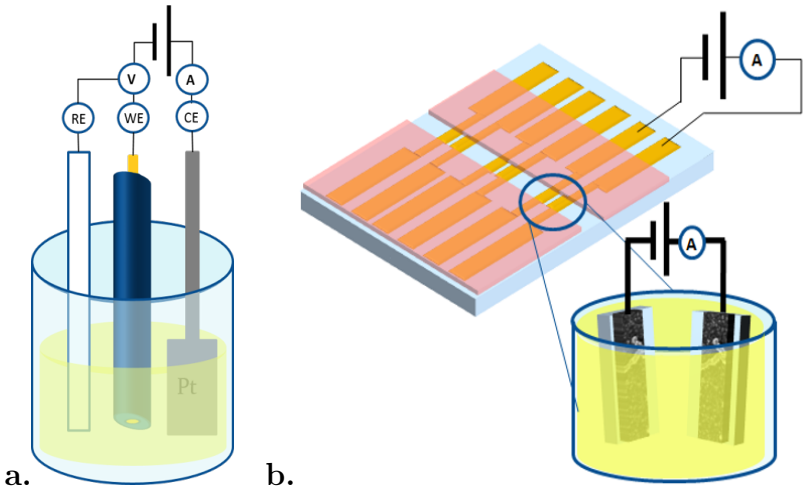

Figure 1.3: a. Three electrode sensor, where the reference electrode (RE) is a silver/ silver chloride electrode, the working electrode (WE) is a gold film electrode covered with polymer-phage film, and the counter electrode (CE) is a platinum plate. b. Two electrode sensor, where one half of the electrode pair is the WE, the other is the RE and CE, and both sides are covered with with polymer-phage film.

experiments using ABs or bovine serum albumin (BSA) as a target analyte were used to verify the incorporation and measurement behaviors. This data shows that different phage types can incorporate into the film as well as keep proper binding. This will be important when exploring multi-channel sensor arrays.

PEI-phage – Second, this part of the chapter describes how PEI-phage films where tested to show phage incorporation, how phage binding ability is maintained, and the transition from a three electrode architecture to a two electrode architecture to a multi-channel senor array.

Lastly, the pros and cons of PEDOT-phage and PEI-phage films are discussed.

1.3 Experimental

Chemicals and Materials – All chemicals were ordered from Sigma Aldrich and used as received unless otherwise specified; 3,4-ethylenedioxythiophene (EDOT, 97%), nitric acid

(70%, $\geq$ 99.999% trace metals basis), lithium perchlorate (99.99%, trace metals basis), iodine, KI, sulfuric acid (99.999%), chromium etchant and Branched Polyethylenimine (B-PEI) MW 25,000, M_n 10,000 ($\leq$ 1% water). Linear Polyethylenimine (L-PEI) and MW 25,000, (Polyscience, Inc) 2%/wt in methanol HPLC grade (J.T. Baker). Nochromix (Godax Laboratories) prepared in sulfuric acid (Macron Fine Chemicals) by the package directions. Positive photoresist Shipley S-1827 and developer MF-319 (Microchem Corporation), Goldpellets (5 N purity, Kurt J. Lesker Co.), and chromium powder (3 N purity, American Elements). Copper conductive tape 12.7mm W x 16.46 m L (Ted Pella) and quick dry top coat clear protectant polish (N.Y.C New York Color). Bovine Serum Albumin (BSA) and Human Serum Albumin (HSA) (Fisher Scientific). Bateriophage M13 specifically modified to bind BSA (BSA-binding phage) provided by Weiss group at UC Irvine. Phosphate buffered saline (PBS 1X, pH 7.4) and Phosphate buffered fluoride (PBF 1X, pH 7.4) were filter-sterilized through a 0.22 m pore size membrane (Corning). It is specified which was used as the run buffer in experiments and storage buffer for phage, BSA, and HSA. Water for all solutions and rinse processes was processed by a Millipore Milli-Q UV system (resistance >18 MΩ cm).

Fabrication of Gold electrode devices used with PEDOT-phage and PEI-phage devices – Gold electrode film devices were fabricated by photolithography, as depicted in Figure 1.4. Starting with a 1 in x 1 in cleaned glass slide (1), a layer of photoresist (PR) was spincoated onto the surface (2), baked in a 90 °C oven for 30 min, then patterned using a contact mask and a 365 nm UV light source, shutter, and alignment stage (Newport, 83210i-line, 1.80 s). The photoresist layer was then developed for 30 s (Shipley, MF-319), and rinsed with Millipore water (3). A 2 nm thick layer of chromium and then 60 nm thick layer of gold were thermally evaporated onto the surface (4). The slides were then submerged in acetone and sonicated to "lift off" gold and photoresist layer (5), acetone was exchanged for fresh acetone and devices were sonicated until all photoresist was removed (6). After "lift off" the 1 in x 1 in slide was cut to separate devices, then plasma cleaned and prepared for sensing by gently sanding the

contact pad of the device and attaching copper electrical tape to the end and applying a clear protectant coating to eliminate current leakage (7). When the protectant coat was dry the device was ready for sensing and placed into a cell holder that further prevents current leakage and exposed only the electrode pads to the run buffer (8).

Electrochemical Impedance Analysis – All Electrochemical Impedance Spectroscopy (EIS) measurements were made using a PARSTAT 2273 potentiostat controlled by POWERSine software (Princeton Applied Research, Oak Ridge, TN). Five consecutive EIS measurements were acquired at a 10 mV voltage modulation amplitude, over 50 data points, spanning 0.1 Hz to 1 MHz, at 0 V versus open circuit.

Fluorescent analysis – Fully fabricated devices were used for these experiments. 20 μl of 5:1000 diluted Dylight 488 Maleimide (Life Technologies) in PBS was pipetted onto the electrode area of the device, to dye phage, then let stand for 30 minutes. The electrodes were then thoroughly rinsed with nano pure water, dried with an air gun, and imaged using an Axioskop 2 MAT Ziess microscope fitted with a FITC filter and an X-Cite series 120 Q mercury arc lamp source. All optical images were taken at 10 x magnification and approximately 30+ images of a single device were compiled by Image Composite Editor to show a full panorama of that device. All fluorescent images were taken using the lowest intensity setting of the light source.

AFM and SEM Analysis – Atomic force microscopy (AFM) topographical and phase traces were acquired on PEI-Phage electrode devices using an Asylum Research MFP-3D AFM equipped with Olympus AC160TS-R3 tips in ambient laboratory air. Scanning electron microscopy (SEM) was performed on PEDOT-phage and PEI-phage electrode device using an FEI Magellan XHR SEM (extreme high-resolution scanning electron microscope) at an accelerating voltage of 1 kV, unless otherwise stated on the micrograph. No metals were sputtered onto the devices for imaging.

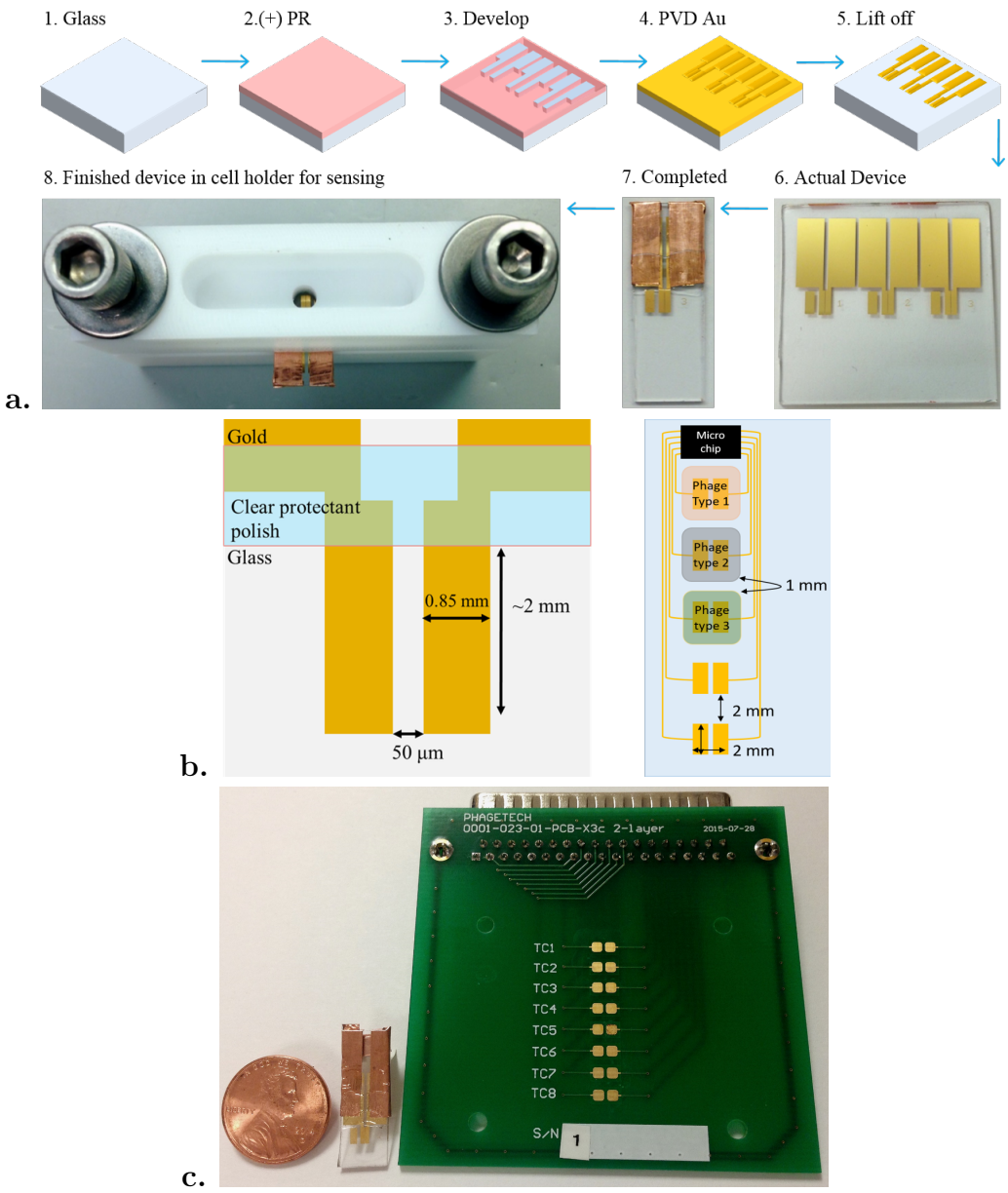

Figure 1.4: a. Fabrication process for single gold electrode devices. b. Dimensions of a single electrode pair and multi channel device. c. Optical image of a real commercially fabricated sensor array.

1.4 Results and Discussion

Fabrication and characterization of PEDOT-phage film electrode devices – PEDOT-phage films were electrochemically polymerized by using cyclic voltammetry [18, 35, 39, 7, 61, 6, 17]. The electrode pair is connected as the WE, and exposed to 1 ml of a 12.5 mM $LiClO_4$, 2.5 mM EDOT solution (plus 3–12 nM phage, for PEDOT-phage films). The RE and CE are only used in growing the films, not in the EIS measurements. The potential is cycled for 9.5 cycles, starting potential (E_0) is 0.4 V and ending potential (E_f) is 1.1 V, as shown in Figure 1.5a. The films are then left overnight to stabilize in PBF run buffer. A SEM of a PEDOT-phage film is shown in Figure 1.5b.

After film electropolimerization impedance measurements are taken by connecting the WE to one side of the electrode pair and the CE and RE both connected to the other side of the electrode pair as shown in Figure 1.3b. These measurements occurred in PBF, then 100 nM negative AB (anti-FLAG) in PBF, then 100 nM positive AB (anti-M13) in PBF, all solutions are 1 ml. After each measurement the electrode is rinsed with PBF three times. EIS provides data for the imaginary impedance (Z_{img}) and real impedance (Z_{re}), which when plotted Z_{img} vs Z_{re} creates a Nyquist plot, shown in Figure 1.6. Three plots show data for each electrode pair, 1) gold, 2) PEDOT-phage 3) PEDOT films. The PEDOT and PEDOT-phage film data are in the same axis range, however the gold data is two orders of magnitude higher, meaning the films reduce the impedance between the electrode pairs. The PEDOT-Phage film pair shows a slightly more elevated impedance than the PEDOT film, this is to be expected from the phage incorporation. In the Nyquist plots it seems that both PEDOT and PEDOT-phage films show an increase to Z_{re} impedance (depicting the resistance portion of the impedance), however the PEDOT-phage shift is larger. The desired outcome of this project is to have the PEDOT-phage film show an elevated signal from anti-M13 and a reduced or negligible signal from anti-FLAG. Further analysis of the data is needed to determine the actual signal from exposure to both antibodies, we do this

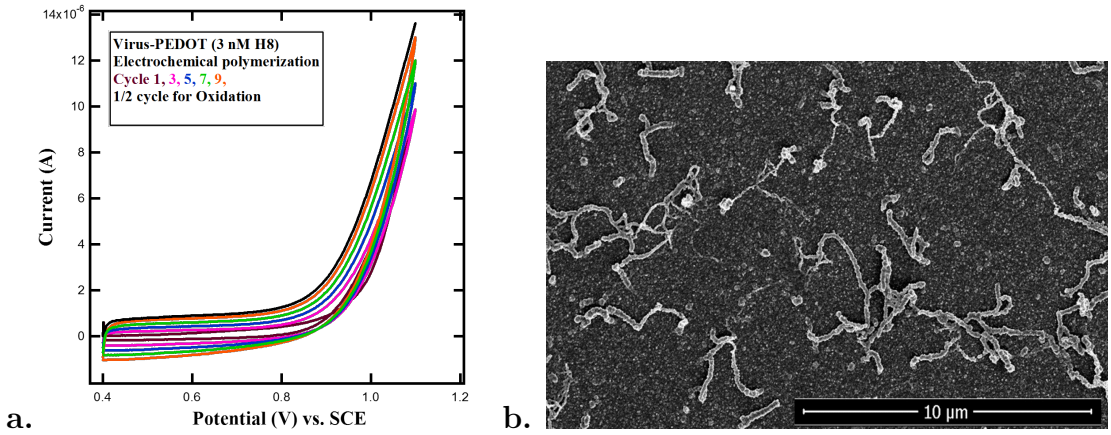

Figure 1.5: a. Cyclic voltamagram of growth cycles. b. SEM for a PEDOT-phage film.

by separately using the Z_{re} and Z_{img} data. Each set is subtracted by an initial impedance (an EIS measurement made in PBF only) and graphed versus frequency. This creates the normalized data, and is expressed as,

$$\frac{\Delta Z_m}{Z_0}$$

where Z_0 is the initial impedance taken in PBF, and ΔZ_m is Z_m-Z_0, where Z_m is the impedance after exposure to antibody.

All EIS data was taken from 0.1 Hz to 1 MHz, however only data from 10 Hz to 0.1 MHz is shown as this is the range of least noise. The normalized data for Z_{re} and Z_{img} versus frequency is shown in Figure 1.7. The Z_{img} data shows that throughout the 10 Hz to 0.1 MHz frequency range the PEDOT-phage film shows an increased signal for anti-M13. This is the desired signal and showing promise for this architecture design. The Z_{re} data also shows an increase for anti-M13 with the PEDOT-phage film, but only in the range of 10 Hz to ∼100 Hz. The PEDOT film shows an increase in signal for the anti-M13 that overlaps the PEDOT-phage signal in frequency's over 100 Hz, indicating signal in the Z_{img} data shows better selectivity than signal in the Z_{re} data.

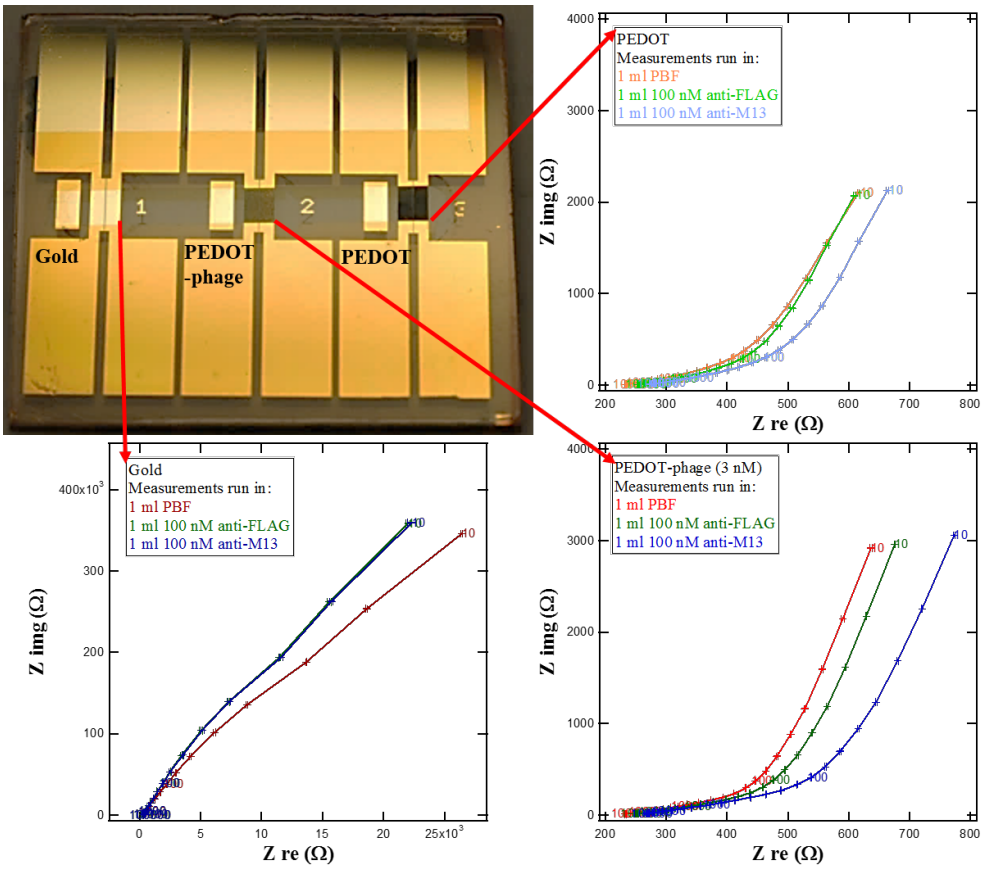

Figure 1.6: Optical image of fabricated device containing three electrode pairs, 1) gold, 2) PEDOT-phage 3) PEDOT films. Nyquist plots for each electrode pair are shown. The PEDOT-phage and PEDOT film Nyquist plots are on the same axis, however the Gold data is two orders of magnitude larger and therefore is plotted on different axis.

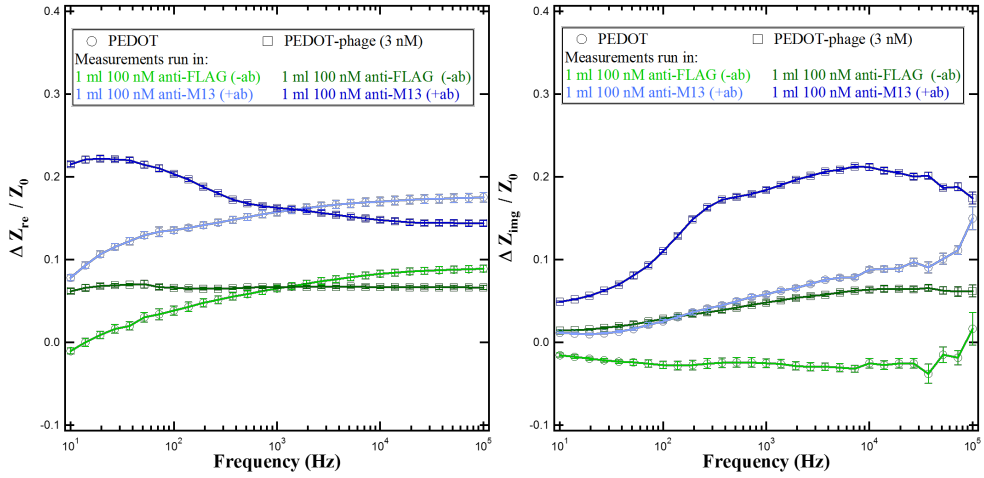

Figure 1.7: Normalized data for Z_{re} and Z_{img} versus frequency.

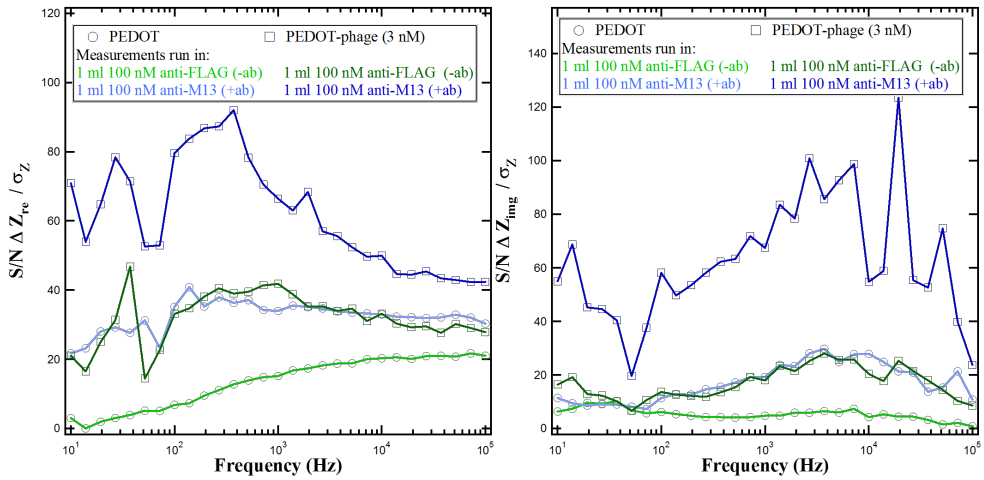

Figure 1.8: Z_{img} and Z_{re} signal to noise ratio plotted versus frequency.

The signal to noise (S/N) ratio for Z_{img} and Z_{re} is expressed as,

$$\frac{\Delta Z_{norm}}{\sigma_{Z_{norm}}}$$

where Z_{norm} is taken from the data above and $\sigma_{Z_{norm}}$ is the standard deviation calculated for the normalized data. The S/N ratio is important as it shows the best frequency to make measurements. This allows future experiments to be run at just a few or even one frequency, reducing the time it takes to make measurements. The S/N ratio is shown in Figure 1.8. The S/N ratio for Z_{img} shows an elevated signal for almost all frequencies, however the best frequencies to make measurements at are 19,307 Hz, or between 2,000 Hz and about 7,000 Hz. In the Z_{re} data the S/N ratio actually helps to separate the anti-M13 signal form the PEDOT-phage film data, and shows that the best frequencies to measure are around 900–1,000 Hz. Optimal frequency can change from phage type and specific analyte, so until these parameters are specified future experiments should measure the entire range of frequencies.

These results show an alternative phage type can replace the PSMA phage type to sense a specific analyte, as well as a working architecture for an array of films that can be exposed to the same solution and have reliable measurements. New experiments are performed to

explore ways to simplify the deposition steps, as well as reduce the amount of phage used. PEDOT-phage films require a large volume of solution for deposition, typically using 50 ml total solution volume of 3–12 nM phage. It is assumed that not all the phage in this solution is incorporated into the PEDOT-phage film, and therefore wasted due to the need for a fresh polymerization solution for each film to ensure consistent film growth. An alternative to electropolymerization deposition is layer-by-layer deposition. Only a small amount is needed to coat the surface of the gold electrode, reducing the amount of solution needed for deposition, as well as reducing the amount of phage wasted in discarded solution.

Fabrication and characterization of PEI-phage film electrode devices – LBL deposition begins immediately after plasma cleaning of the bare gold electrode. The first generation (1G) devices started with a PEI layer, 10 μL of a 2% by weight L-PEI solution in methanol was pipetted onto each device and left to dry in open air. The device was then rinsed thoroughly with Millipore water, dried with an air gun, and then a phage layer, 10 μL of 86 nM phage solution is pipetted on to the device and left to dry in open air. The devices are again rinsed thoroughly with Millipore water and dried with an air gun. Second generation (2G) devices add PEI and phage layers in hopes of increasing the sensing signal. A second PEI layer is added using B-PEI. L-PEI is not soluble in water and phage can not survive in organic solvents, therefore B-PEI is used as the second PEI layer. However, L-PEI showed the best PEI-gold interaction, requiring the first layer of PEI on gold to be L-PEI and ensuring complete PEI coverage on the gold electrode. For 2G devices, 10 μL of a 2% by weight B-PEI solution in water is pipetted onto each device, left for 1 hour, and rinsed with water. A second phage layer of 10 μL of 86 nM phage solution is pipetted on to the device and left for 1 hour, then rinsed. These devices are not dried out after the first layer to prevent shrinking and swelling of the B-PEI layer. These steps are repeated to make a total of three PEI layers and three phage layers. Third generation (3G) devices alter the phage layer by repeating it three times after each PEI layer to increase phage loading and attempting to make evenly covered devices.

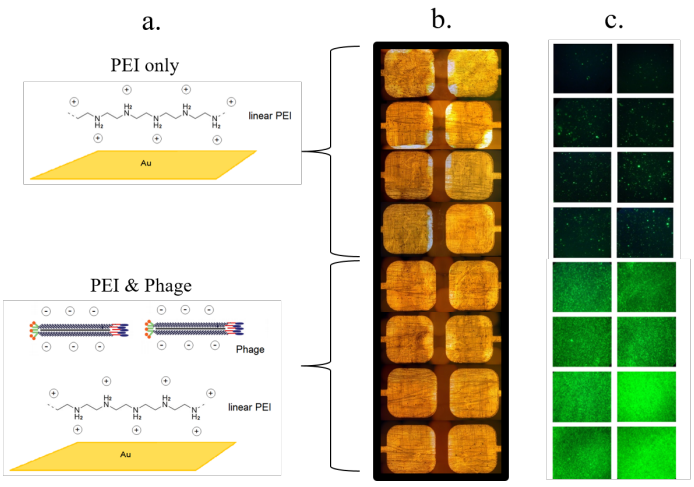

Figure 1.9: a. Schematic of layer-by-layer deposition for PEI only and 1G PEI-phage films. b. Compiled optical images of entire multi-channel biosensor, top half are PEI only films and bottom half are 1G PEI-phage films. c. Compiled fluorescent images of multi-channel biosensor showing phage presence; top half PEI only films limited fluorescent emission and bottom half PEI-phage films, bright green, large fluorescent emission.

After fabrication the devices were set in PBS for 1 hour to allow equilibrate before impedance measurements were taken. The schematic in Figure 1.9a shows electrostatic force attraction absorption of alternating polyanions (phage) and polycations (PEI). L-PEI and B-PEI were both used as the polycation layer in PEI-phage devices, however for diagram simplification only L-PEI is show in Figure 1.9a.

In comparison to the 50 ml of 3–12 nM phage needed for PEDOT-phage deposition, the same amount of phage needed for a PEI-phage device would only make 0.034 nM phage solution. LBL deposition greatly reduces the amount of phage used and is much easier to perform in commercial mass production.

Confirmation of phage presence was performed by fluorescent imaging. Close up panorama images of a 1G multi channel device, from Figure 1.4c is shown in Figure 1.9. Bright field optical image is shown in Figure 1.9b and fluorescent image in Figure 1.9c. The top half of the device was layered with PEI only and the bottom half with 1G PEI-phage. These fluorescent images shows a clear difference when phage is present. Figure 1.10 shows two

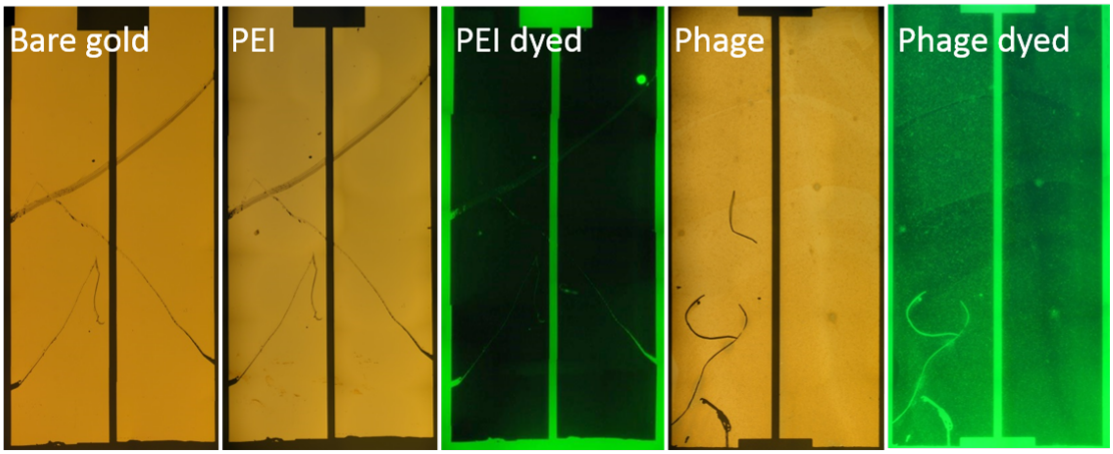

Figure 1.10: Optical and florescent images of two 1G single gold devices after layer-by-layer deposition of PEI (first three images) and PEI-phage (last two images), respectively. Dark lines are scratches in the gold electrode created to help compile images to make a panorama, also to show that the same device was used in the optical and fluorescent images.

1G electrode pair gold devices, in bright field and fluorescence, PEI only and 1G PEI-phage, respectively. These images again show clear differences when phage is present.

Other characterization tools, AFM and SEM, were performed on 1G electrode pair gold devices and are shown in Figures 1.11 and 1.12. AFM was performed on three different 1G electrode pair gold device films, a. gold, b. PEI, and c. 1G PEI-phage, showing the change in roughness when phage is present and confirming the presence of phage in the 1G PEI-phage film. SEM was performed on two 1G electrode pair gold devices, a. gold and b. 1G PEI-phage, confirming again the presence of phage in the 1G PEI-phage film. PEI only data is not shown due to a lack of difference between gold only and PEI only devices.

To confirm the phage will bind while in a PEI-phage film, anti-M13 antibody (+ab), which binds to any phage type, was used as the target and three electrode experiments, as shown in Figure 1.3a, were performed before experimenting with a target protein and two electrode devices. Two controls, bovine serum albumin (BSA) and anti-FLAG antibody (-ab), were used to verify there is no non-specific binding to the films. Normalized data for 1G PEI-phage films is shown in Figure 1.13. While the Z_{re} data does not show much change, there

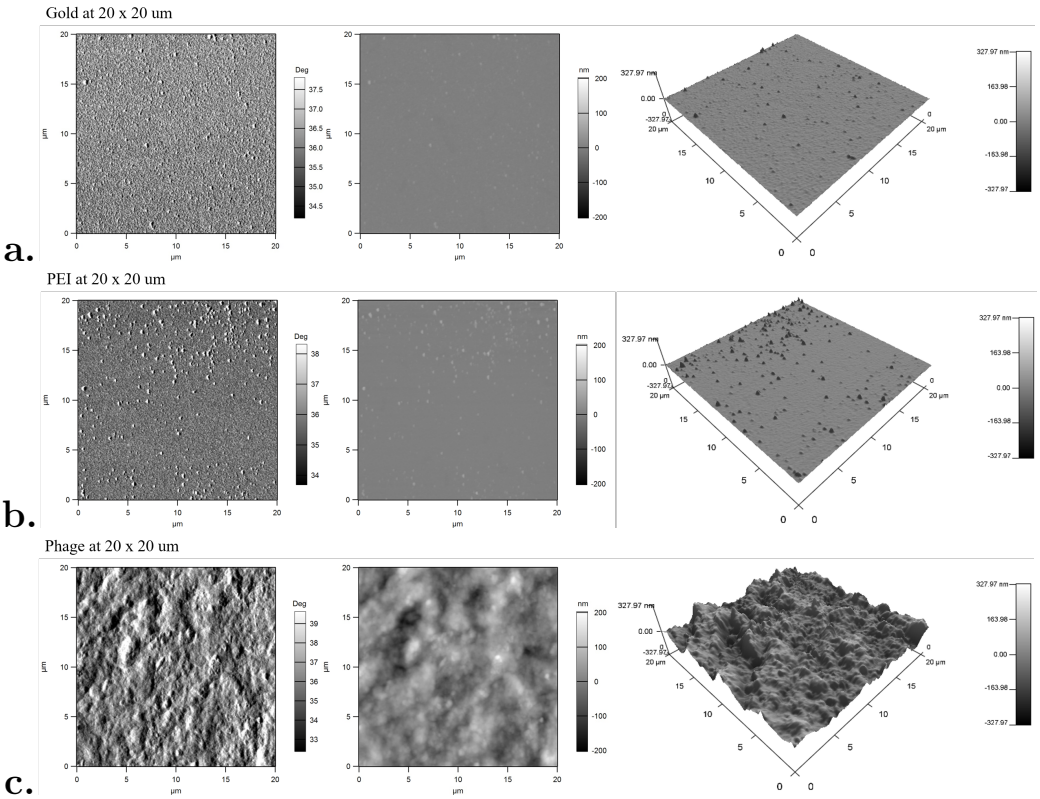

Figure 1.11: AFM of three 1G electrode pair gold devices; a. clean gold, b. PEI, and c. 1G PEI-phage.

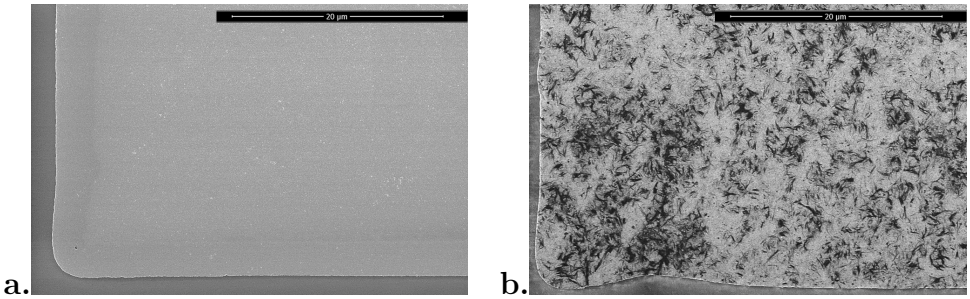

Figure 1.12: SEM of two 1G electrode pair gold devices; a. clean gold and b. 1G PEI-phage.

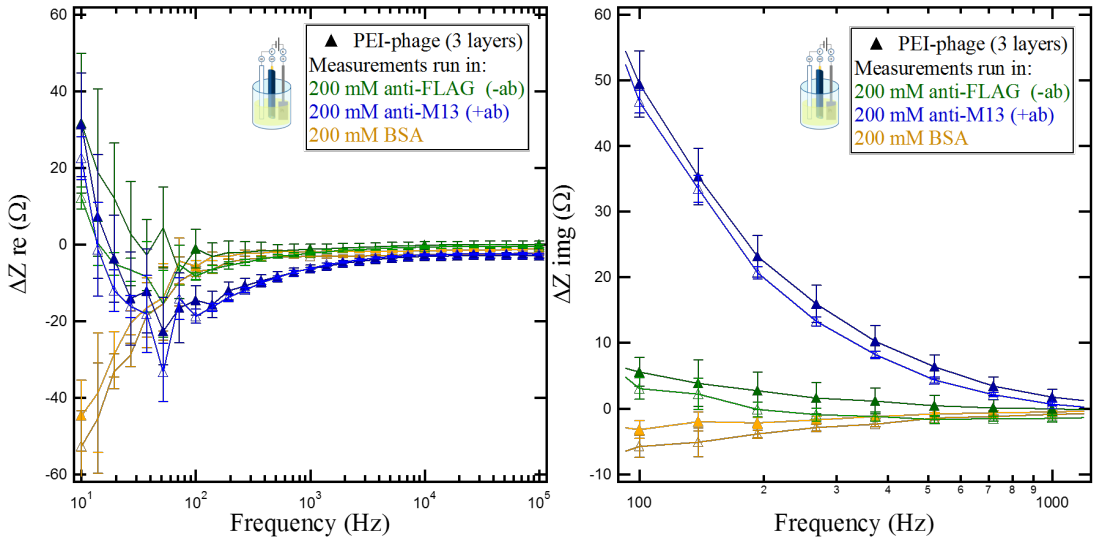

Figure 1.13: Normalized Z_{re} and Z_{img} data for a 1G PEI-phage film using a three electrode set-up. EIS was taken from 10–100,000 Hz, however Z_{img} data has been zoomed in to show optimal frequencies.

is signal increase in the Z_{img} data, confirming the phage retains binding properties while in a PEI-phage film. The PEDOT-phage device also showed a greater signal in Z_{img}, meaning the PEI-phage devices are acting similar to previous phage film devices.

Even though phage binding was confirmed, additional experiments were performed to find the greatest phage loading, confirm protein binding, and to determine if the signal would increase by using a two electrode set-up like the one shown in Figure 1.3b. Fabrication steps for these experiments are described above as 2G and 3G devices. Normalized data for 3G electrode pair gold devices, using a two electrode set-up, is shown in Figure 1.14. The target protein BSA and control protein HSA were investigated as positive and negative responses against BSA-binding phage. 3G electrode pair gold devices are exposed to 2 mL of PBS solution and allowed to equilibrate, as described above. Two initial EIS measurements of PBS only were taken to verify lack of signal from solution change, then 2 mL of 200 nM of each target in PBS were exposed to different 3G electrode pair gold devices. Separate, fresh devices were used for positive and negative exposures, shown in Figure 1.14, to ensure any signal change was from a single protein. When exposed to BSA the normalized data showed

an increased signal for Z_{re} and a decrease in signal for Z_{img}. This data was inconsistent with the observations of the three electrode experiments above, indicating that the two electrode experiments might rely on different mechanisms for sensing. When exposed to HSA the normalized data showed a mild signal for Z_{re} and a decrease in signal for Z_{img}, however the signal was much smaller than that for BSA. The Z_{re} HSA data falls with in the margin of error when the solution is changed, under 50 Ω, but the Z_{img} is much larger than the change due to solution change. Further experimentation is need to explore the mechanism and reasons for non-specific binding signal and is not discussed in this work.

The last modification done in this work was to test reliability and constancy of multi-channel two electrode device (Figure 1.4c). Normalized data for 2G electrode pair gold devices, using a two electrode set-up, is shown in Figure 1.15. Unfortunately, this data does not concur with the data from the non-multi-channel two electrode experiments, as there is no signal in the Z_{re} or Z_{img} data. Again, further experimentation is need to explore the reasons for the lack of signal and is not discussed in this work. These experiments show inconclusive data towards attempting to make a simpler fabrication method for phage based sensors. Another problem encountered with PEI-phage films was inconsistent phage coverage as shown in Figure 1.16. These fluorescent images show the variation in phage cover for three different films. The drying steps allow the salt from the PBS solution that the phage is stored in to form salt crystals and cause areas of high and low phage coverage. Further experimentation attempted to solve this issue by using an automated micro pipetting system. This data is not shown or discussed here, but it can be said that so far these attempts have been unsuccessful due to pipette tip clogging from the methanol PEI solution and from the size of the phage.

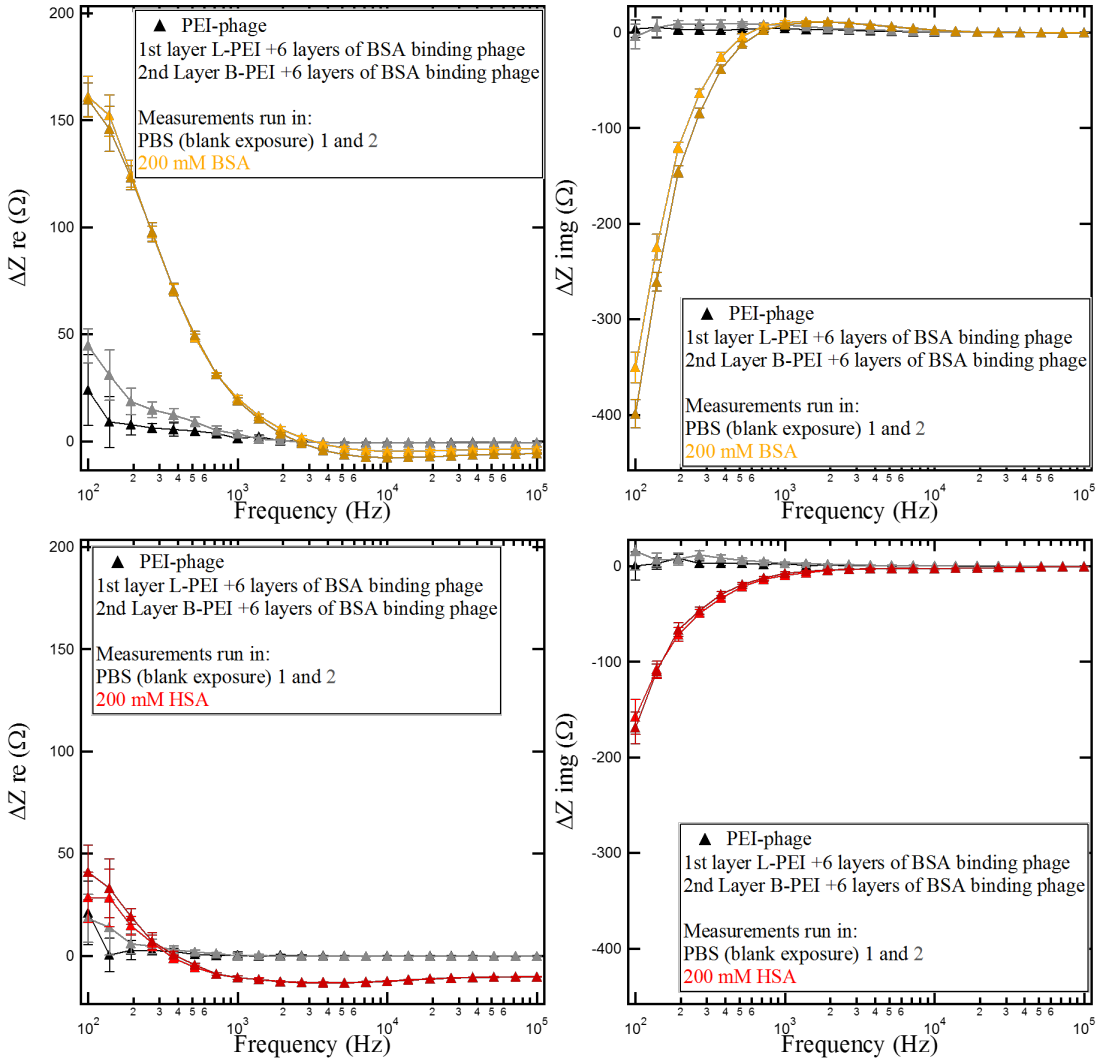

Figure 1.14: Normalized Z_{re} and Z_{img} data, using a two electrode set-up, for 3G PEI-phage films that were exposed to target protein BSA (in gold) and control protein HSA (in red). EIS was taken from 10–100,000 Hz, however data has been zoomed in to show optimal frequencies.

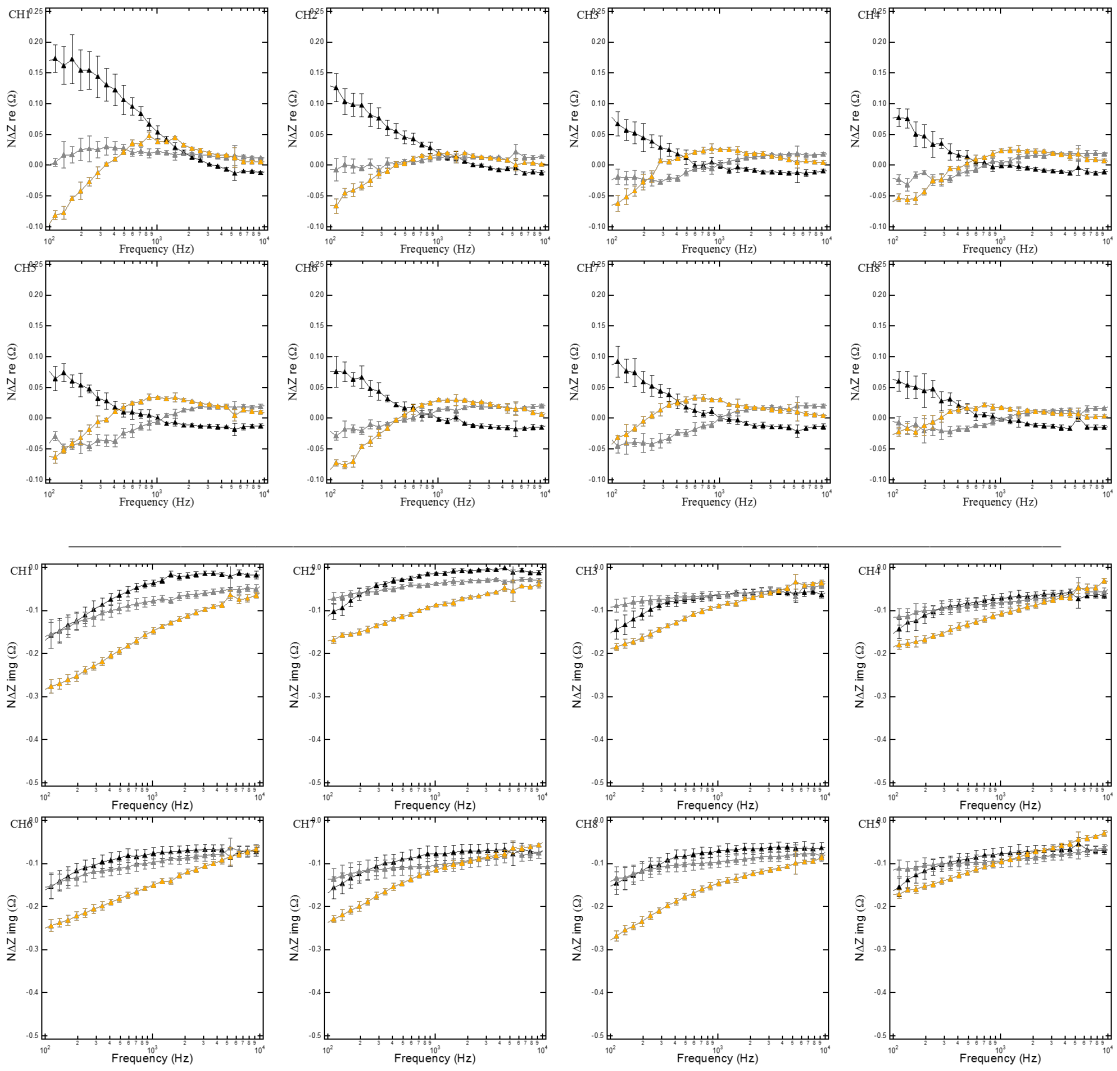

Figure 1.15: Normalized Z_{re} and Z_{img} data is shown for a multi channel set-up. This contains eight separate films as shown in Figure 1.4c., each graph is labeled in the top left corner with the channel number which corrilates to the TC number on the device in Figure 1.4c. These films were fabricated using the 2G PEI-phage film procedures and were exposed to 200 nM, target protein BSA exposures are in gold and PBS-only exposures are in black. EIS was taken from 10–100,000 Hz, however data has been zoomed in to show optimal frequencies.

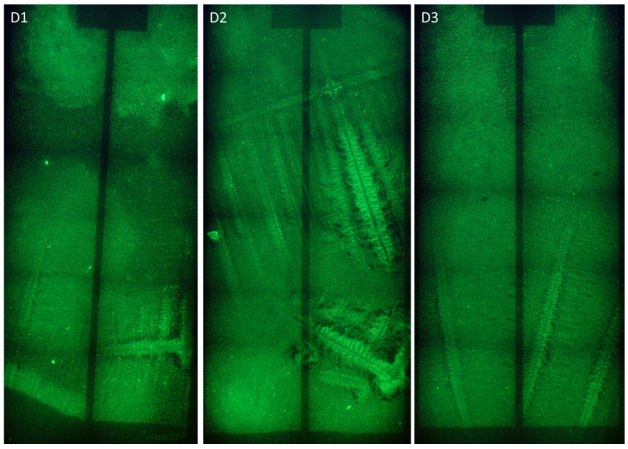

Figure 1.16: Optical image and Florescent image of three different single gold devices showing the variation in phage loading.

1.5 Conclusions

This chapter has reviewed methodology steps designed to optimize a phage-based protein sensor. Steps to make the sensor less expensive were successful by removing the CE and RE by using a two electrode set-up. It was also determined that various phage types can be incorporated into a film while maintaining binding properties. However, these experiments were not successful at optimizing sensitivity and reducing fabrication steps. Experiments performed to address sensitivity and fabrication revealed issues that need to be addressed in future research.

Chapter 2

Iron(III) Detection

2.1 Abstract

Arrays of nanowires of an electronically conductive polymeric affinity medium tailored to the detection of Fe(III) are prepared, and their properties for detecting Fe(III) are evaluated. This polymeric affinity medium consists of poly(3,4-ethylenedioxythiophene) or PEDOT into which an iron chelator, deferoxamine (or DFA), has been doped during the polymerization process. PEDOT-DFA nanowires are potentiostatically deposited from a solution containing both EDOT and DFA using lithographically patterned nanowire electrodeposition (LPNE). The through-nanowire electrical resistance of PEDOT-DFA nanowires is measured as a function of the Fe(III) concentration. In parallel with measurements on PEDOT-DFA nanowire arrays, the electrochemical impedance of PEDOT-DFA films is characterized as a function of the Fe(III) concentration and the frequency of the impedance measurement in order to better understand the mechanism of transduction. PEDOT-DFA nanowires detect Fe(III) from 10^{-4} M to 10^{-8} M with a limit-of-detection of 300 pM (calculated) and 10 nM (measured).

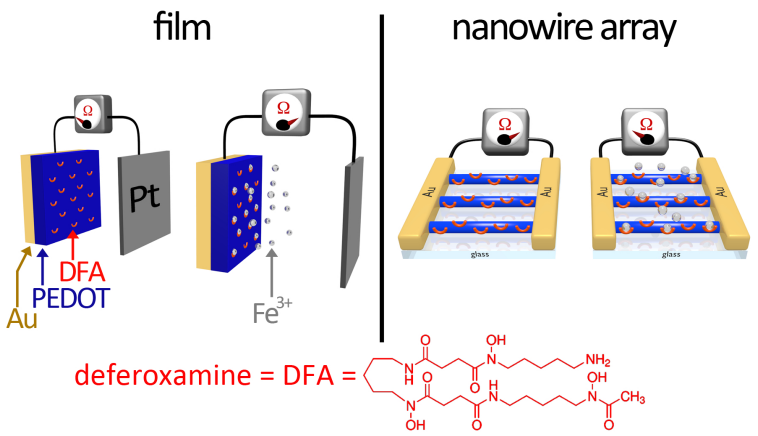

Figure 2.1: Two sensor architectures for transducing the binding of Fe(III) to PEDOT-DFA: Films (left) and nanowires (right).

2.2 Introduction

This chapter describes a polymeric nanowire-based chemiresistor capable of detecting iron(III) at nanomolar concentrations in aqueous solution. We ask the question: Can one entrain a metal chelator into a conductive polymer nanowire to produce a chemiresistor that possesses the ability to selectively detect a metal ion? To answer this question, we attempt to do the following: First, to directly compare films and nanowires composed of a simple polymeric affinity medium consisting of poly(3,4-ethylenedioxythiophene) or PEDOT into which an iron chelator, deferoxamine (or DFA), has been doped during the polymerization process (henceforth: PEDOT-DFA). Second - to exploit the measurements made on both sensor architectures to derive a consistent picture of the mechanism of transduction. Third, to develop a sensitive, selective, and extremely simple sensor for Fe(III) in aqueous solution. We are not aware of existing chemiresistors - either nanowire or film based - that are capable of this measurement. Moreover, to date, ion-selective electrodes (ISEs) for Fe(III) have so far achieved a limit-of-detection of $\approx 10^{-6}$ M [57, 32, 20, 40] - a concentration well above that attainable for other metal ions using this technology, [34, 5, 49].

The history of this problem is as follows: The electropolymerization of poly(pyrrole) was discovered by Diaz and coworkers in 1979 [16] and the electropolymerization of poly(thiophene) was first reported by Kaneto *et al.* in 1982 [23]. On the heels of these discoveries, the application of conductive polymers on electrodes to analytical problems began to be explored. In 1989, Moutet [15] described the use of functionalized pyrroles to enhance the weak affinity of polypyrrole to metal ions, imparted by its amine functionalities. Adducts of bipyridinium and pyrrole, for example, produced a polypyrrole derivative that showed strong, reversible binding of Ru(II).[15] Other examples of this approach followed [29, 27]. But it was soon demonstrated by Shui and coworkers [48] that covalently grafting a ligand onto the polymer backbone was not required, ionophores such as bathophenanthroline disulfonate (BPD) could be entrained in the polymer during electropolymerization, dramatically simplifying the process of preparing these films. Square-wave voltammetry was then used to assess the partitioning of Cu^{2+} into their doped films and correlated Cu^{2+} loading into the film with its concentration in solution. In all of the work to this point, films of the conducting polymer containing an ionophore, or films of nanowires composed of ionophore-doped conductive polymer [28], were electrochemically interrogated, but such nanowires were not configured as chemiresistors. In 2009, Myung, Mulchandani and coworkers [4, 21] performed the first experiments in which ionophore-doped nanowires were configured as chemiresistors. Using nitrilotriacetic acid (NTA)-doped polypyrrole nanotubes prepared using template synthesis, Cu^{2+} was detected, [4]. In that paper, the through-nanowire resistance of the polypyrrole nanotube, measured using two electrical contacts, decreased upon exposure to Cu^{2+}. Subsequently, Lee and coworkers doped poly(pyrrole) nanowires with a tripeptide ionophore to obtain chemiresistive nanowires also for the detection of Cu^{2+}. FETs have been prepared from polypyrrole and polyaniline nanowires [56, 47] but they have not yet been applied to the problem of metal ion sensing. To our knowledge and surprise, these two papers constitute the full extent of the literature pertaining to conductive polymer nanowire chemiresistors for detecting metal ions.

Because metal ions are both small and highly charged, they represent ideal candidates for field-effect transistor (or FET)-based nanowire sensors derived from semiconductor nanowires that are functionalized with ionophores. Predictably, a somewhat larger number of papers have been devoted to exploring these devices for metal ion detection (Table 1), [14, 10, 11, 31, 19, 50] . Two motivations for pursuing conductive polymer sensing systems are, first, the inherent simplicity, reliability, and low cost of the chemiresistor device architecture and second, conductive polymer nanowires prepared by electrodeposition can be lithographically patterned onto the surfaces of dielectrics like glass and polymers [7, 51, 6, 38].

In this chapter, PEDOT-DFA films are potentiostatically deposited from a solution containing both EDOT and DFA. PEDOT-DFA nanowires are prepared using lithographically patterned nanowire electrodeposition (LPNE), [33, 59, 60]. The through-nanowire electrical resistance of PEDOT/DFA nanowires and the electrical impedance of PEDOT/DFA films are characterized as a function of the Fe(III) concentration and, in the case of films, the frequency of the impedance measurement. Arrays of PEDOT-DFA nanowires detect Fe(III) from 10^{-8} M to 10^{-4} M with a limit-of-detection ($\mathrm{LOD}_{Fe(III)}$) of 300 pM (calculated) or 10 nM (demonstrated). This represents a significantly lower $\mathrm{LOD}_{Fe(III)}$ than has been obtained using ion-selective electrodes, [57, 32, 20, 40].

2.3 Experimental

Materials - Positive photoresist Shipley S-1808 and MF-319 were purchased from Microchem Corporation. Gold pellets (5 N purity, Kurt J. Lesker Co.) and chromium powder (3 N purity, American Elements) were used for the evaporation of films. Deferoxamine-mesylate salt ($\geq$92.5%), 3,4-ethylenedioxythiophene (97%), sodium nitrate ($\geq$99.999%, metals basis), iron (III) nitrate nonahydrate (99.99%, trace metals basis), zinc nitrate hydrate (99.999%,

trace metals basis), nitric acid (70%, ≥99.999% trace metals basis), lithium perchlorate (99.99%, trace metals basis), iodine, KI, sulfuric acid (99.999%), and chromium etchant were all used as received from Sigma-Aldrich. Milli-Q UV water ($\rho > 18$ MΩ.cm) was used for the preparation of all solutions and for the rinsing of all samples. *Synthesis of PEDOT-DFA films* - Circular gold electrodes (1.6 mm diameter, BASi Inc.) were manually polished using a polishing microcloth (Buehler) in conjunction with diamond polishing pastes of decreasing particle sizes beginning with 1 μm, and proceeding to 0.5 μm and 0.25 μm (Ted Pella). Polished electrodes were then cleaned by sonication in Milli-Q water for 10 min. The electrodes were then preconditioned by cycling from 0.3 to 1.5 V vs. saturated calomel electrode (SCE) at 100 mV/s in 0.1 M H_2SO_4 for 15 cycles using a Gamry Series G 300 potentiostat. A flame-annealed platinum foil counter electrode was wrapped around the polymer barrel of the polished gold electrode, as previously described. These electrodes were then placed in the PEDOT-DFA plating solution (1 mM DFA, 5 mM EDOT, 12.5 mM $LiClO_4$). Electropolymerization occurred by cycling between 0.4 and 1.1 V vs. SCE for 15.5 cycles at a scan rate of 20 mV/s. Synthesized films were rinsed in Milli-Q water and immediately transferred into 0.1 M $NaNO_3$, 5 mM HNO_3 solution.

Electrochemical Impedance Spectroscopy (EIS) - Freshly synthesized PEDOT-DFA films were equilibrated in the 0.1 M $NaNO_3$, 5 mM HNO_3 solution (pH = 2.9) for 20 min and then transferred into $Zn(NO_3)_2$, 0.1 M $NaNO_3$, 5 mM HNO_3 solution with pH = 2.9. The probable chemical state of Zn(II) in aqueous solution at this pH is $Zn(H_2O)^{2+}$, [41]. Five consecutive EIS were acquired using a Gamry Series G 300 potentiostat. A 10 mV voltage modulation amplitude was used in these measurements, and 33 data points were acquired spanning 10 to 100,000 Hz at 0.0 V vs. open circuit potential. The electrode was incubated in the Zn^{2+} solution for 20 min. Five EIS were acquired; the electrode was then rinsed three times with 0.1 M $NaNO_3$, 5 mM HNO_3 and this process was repeated with $Fe(NO_3)_3$ 0.1 M $NaNO_3$, 5 mM HNO_3 solutions also with pH = 2.9. The probable chemical state of Fe(III) in aqueous solution at this pH is $FeOH(H_2O)_2^{2+32}$ [41] which has been proposed to dimerize,

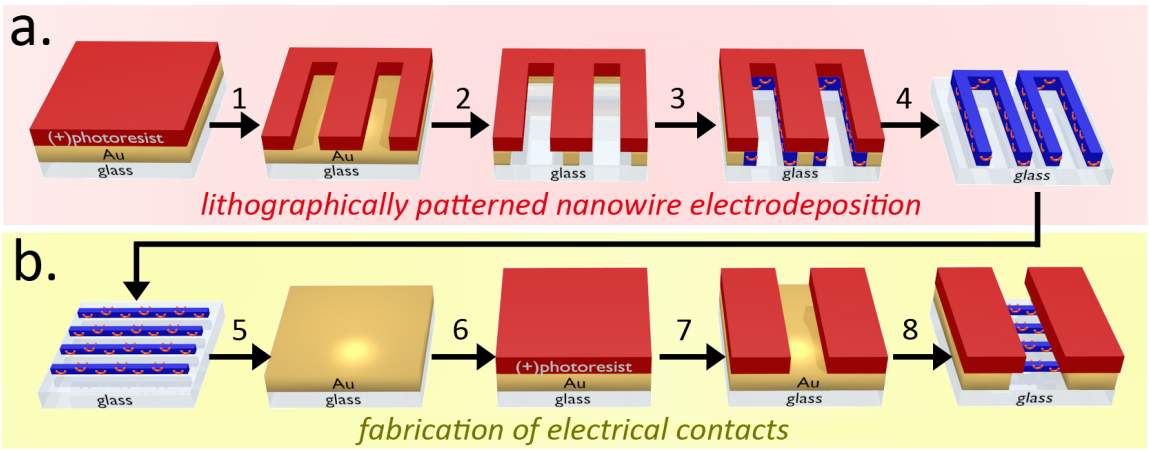

Figure 2.2: Process flow for the preparation of PEDOT-DFA nanowires, and chemiresistors derived from them. a) Preparation of PEDOT-DFA nanowire arrays using lithographically patterned nanowire electrodeposition (LPNE) c,d). The individual steps are described in the text. b) Preparation of electrical contacts on top of PEDOT-DFA nanowire arrays. Each process step is described in the text.

[44]. *Fabrication of PEDOT-DFA nanowire devices* - Arrays of PEDOT-DFA nanowires were prepared using lithographically patterned nanowire electrodeposition (LPNE), [33, 59, 60]. In previous work, we have employed LPNE to prepare arrays of pure PEDOT nanowires, [51] as well as nanowires composed of a composite of M13 virus particles and PEDOT [6]. The LPNE procedure employed here, summarized in Figure 2.2, enabled the preparation of several thousand, linear, parallel, PEDOT-DFA nanowires on a glass substrate. This process first required thermal evaporation of a chromium adhesion layer, followed by a 50 nm layer of gold (Figure 2.2a left-most image). A layer of positive photoresist was spin-coated onto the surface and baked in a 90°C oven for 30 min. Using a contact mask with a 365 nm UV light source, shutter, and alignment stage (Newport, 83210i-line, 2.40 s), the photoresist layer was patterned and then developed for 20 s (Shipley, MF-319), and rinsed with Milli-Q water (Figure 2.2a, step 1). The exposed gold was removed using a solution of KI and I_2 for 15 seconds to produce horizontal trenches below the photoresist edges (Figure 2.2a, step 2).

The exposed chromium was removed using a chromium etchant solution. Using the gold edges within the horizontal trenches as the working electrode in a three-electrode cell, the PEDOT-DFA nanowires were electropolymerized from aqueous 1 mM DFA, 5 mM EDOT, 12.5 mM $LiClO_4$ by cycling from 0.4 to 1.1 V vs. SCE for 9.5 cycles (Figure 2.2a, step 3). The remaining photoresist was removed by rinsing with acetone followed by the complete removal of gold with the solution of KI and I_2 exposing an array of several thousand PEDOT-DFA nanowires (Figure 2.2a, step 4).

The procedure for fabrication of the electrical contacts is shown in Figure 2.2b. Electrical contacts were made to the nanowires by first thermally evaporating first a chromium adhesion layer and then a 70 nm gold layer (Figure 2.2b, step 5). The gold was coated with a layer of (+)-photoresist (Figure 2.2b, step 6) and was patterned to produce a 25 μm gap (Figure 2.2b, step 7). The exposed gold was etched with solution of KI and I_2 and the chromium was etched with chromium etchant (Figure 2.2b, step 8). After exposure of a strip of The photoresist was left on the remaining gold to protect the contacts from exposure to solution. Each nanowire in the parallel array had a rectangular cross section, in which the duration of the electrodeposition and the thickness of the gold layer dictated nanowire widths ($\sim$750 nm) and heights ($\sim$50 nm), respectively. These nanowire arrays were characterized using an FEI Magellan XHR SEM (field-emission scanning electron microscope) at a low accelerating voltage of 2.00 keV to minimize beam damage to the polymer nanostructures. Iridium was sputtered onto the nanowires prior to imaging.

Resistance measurements - The electrical resistance of an array of PEDOT-DFA nanowires was measured in order to transduce the binding ofFe(III) to the nanowires. Connections were made to the gold contacts and the array was placed in a sample holder with a 3.5 mm opening where the wires were exposed to the solutions. The sample holder was filled with 0.1 M $NaNO_3$, 5 mM HNO_3 and three consecutive cyclic voltammograms were collected by scanning from -0.5 to 0.5 V at 100 mV/s. The solution was replaced with solutions contain-

ing increasing concentrations of $Zn(NO_3)_2$ or $Fe(NO_3)_3$ and the scans were repeated. The resistance was calculated at E_{app} = -0.5 V.

2.4 Results and Discussion

Fabrication and characterization of PEDOT/DFA films and nanowires. Films and nanowires of PEDOT-DFA were electrodeposited using the same procedure involving scanning the potential the gold working electrode from +0.40 V to +1.1 V vs. SCE in aqueous 12.5 mM $LiClO_4$, 5 mM EDOT, 1 mM DFA at 20 mV/s for 15.5 cycles (films) and 9.5 cycles (nanowires)(Figure 2.3b,d). Films were prepared at 1.6 mm diameter gold disk electrodes (Figure 2.3a) while nanowire electrodeposition occurred at a gold electrode within a template prepared using the LPNE method [33, 59, 60] (Figure 2.3b). For both films and nanowires, the EDOT oxidation current increased with successive scans with (Figure 2.3a,c) and without (Figure 2.3b,d) DFA present in the deposition solution. This is consistent with a progressively increasing electrode area associated with the deposition of a porous, electronically conductive PEDOT-DFA layer - as we have previously reported [7, 51].

The addition of 1 mM DFA to the deposition solution reduced EDOT oxidation currents to 40% (film) and 80% (nanowires) of their values in DFA-free solutions (Figure 2.3). During electrodeposition, capacitive background currents in the potential range from +0.40 V to +0.80 V are reduced in the presence of DFA relative to DFA-free solutions. Both of these observations demonstrate a reduced rate of polymer deposition in the presence of 1 mM DFA than in the EDOT-only deposition solution.

An array of PEDOT-DFA nanowires on glass, patterned at an interwire pitch of 10 μm (Figure 2.4a), are electrically addressed using two evaporated gold contacts that are spaced

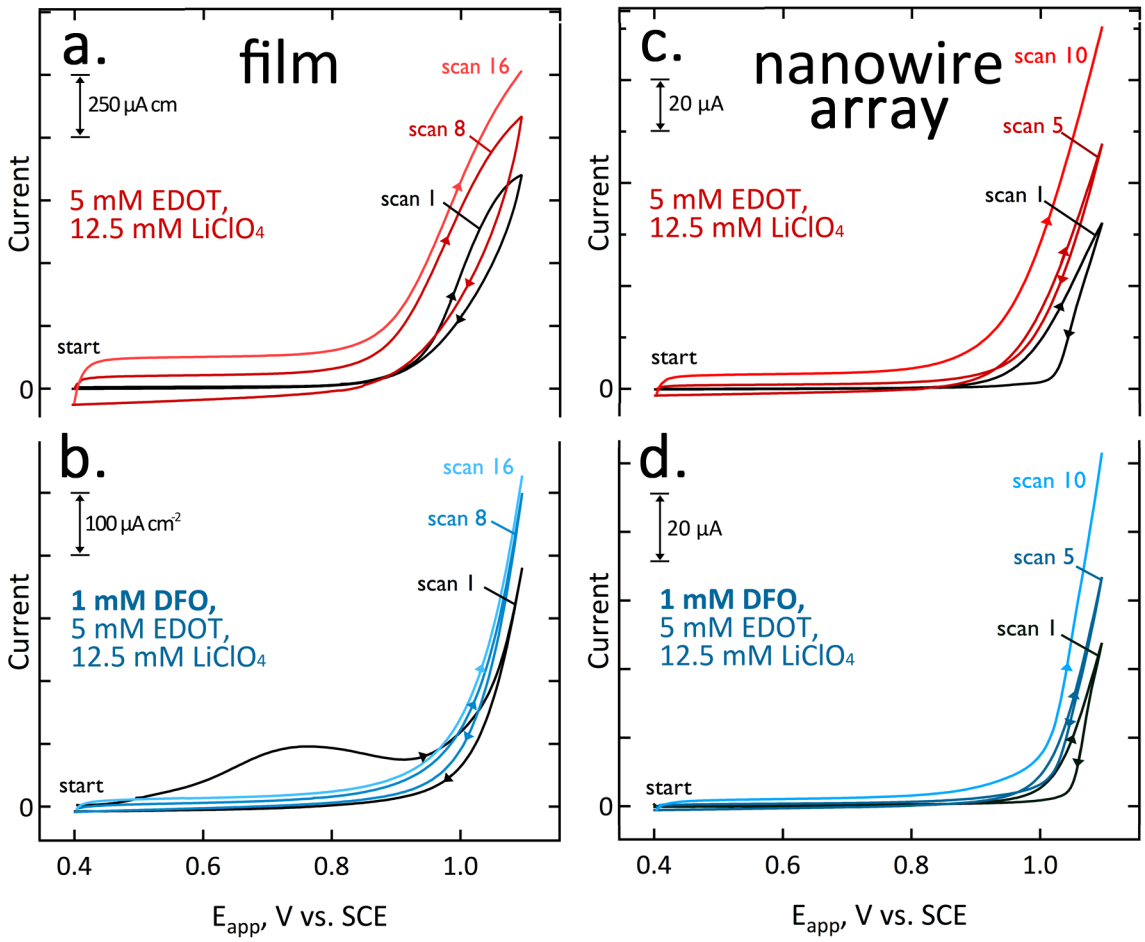

Figure 2.3: Electrodeposition of PEDOT, and PEDOT-DFA. a,b) Electrodeposition of films of PEDOT (a) and PEDOT-DFA (b) on a gold electrode. c,d) Electrodeposition of nanowires of PEDOT (c) and PEDOT-DFA (d) within a LPNE template with a gold edge electrode. All scans were terminated at +1.1 V in order to produce fully oxidatively doped PEDOT having the maximum electronic conductivity. All scan rates 20 mV/s.

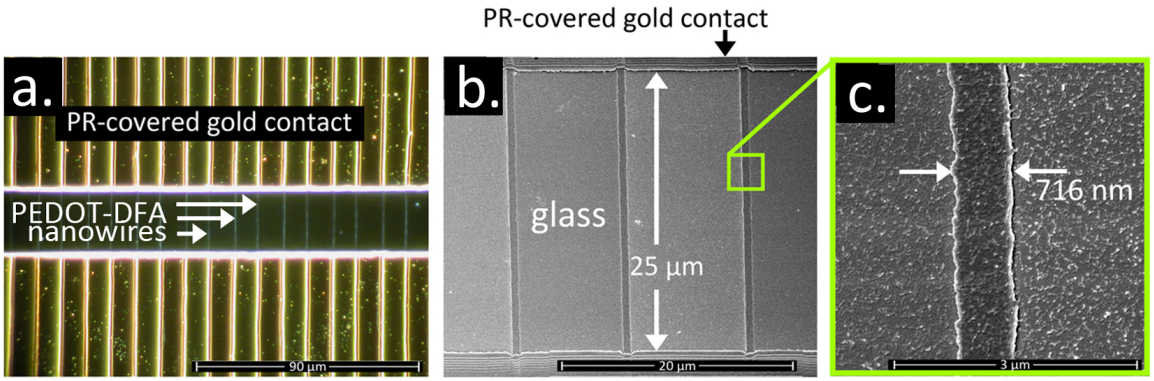

Figure 2.4: Images of PEDOT-DFA nanowires. a) Darkfield optical micrograph of an array of electrodeposited PEDOT-DFA nanowires on glass spanning a 25 μm gap between evaporated gold electrical contacts prepared by the procedure depicted in Figure 2.2. b) SEM micrograph of three PEDOT-DFA nanowires on glass spanning a 25 μm gap between evaporated gold electrical contacts, c) An SEM micrograph showing a single PEDOT-DFA nanowire on glass. All nanowires are ≈50 nm in height.

by 25 μm (Figure 2.4b). Each nanowire has a ribbon morphology with a width of ≈700 nm and a height of 50 nm (Figure 2.4c). The total number of nanowires in the arrays used for sensing was 200.

Detection of Fe(III) by PEDOT/DFA films. The surface texture of films of PEDOT (Figure 2.5a) and PEDOT/DFA (Figure 2.5b) prepared using 16 volumetric scans are indistinguishable, showing texture on a 500 nm - 1.0 μm scale in both cases. The voltammetry of these films is also similar (Figure 2.5c, red and pink traces) but the capacitive current envelope seen over the entire potential window from +0.40 V to +0.80 V is larger by 20-30% for pure PEDOT films suggesting that these films possess a higher wetted surface area as compared with PEDOT/DFA films. This observation is consistent with the observed depression of the polymerization currents seen in the presence of DFA in the deposition voltammograms of Figure 2.3a. DFA impedes the electropolymerization of PEDOT. Moreover, no voltammetric wave is seen corresponding toFe(III) reduction and reoxidation after equilibration of PEDOT or PEDOT/DFA films in solutions containing 10^{-4} MFe(III), the highest concentration explored in this study. (Figure 2.5c)

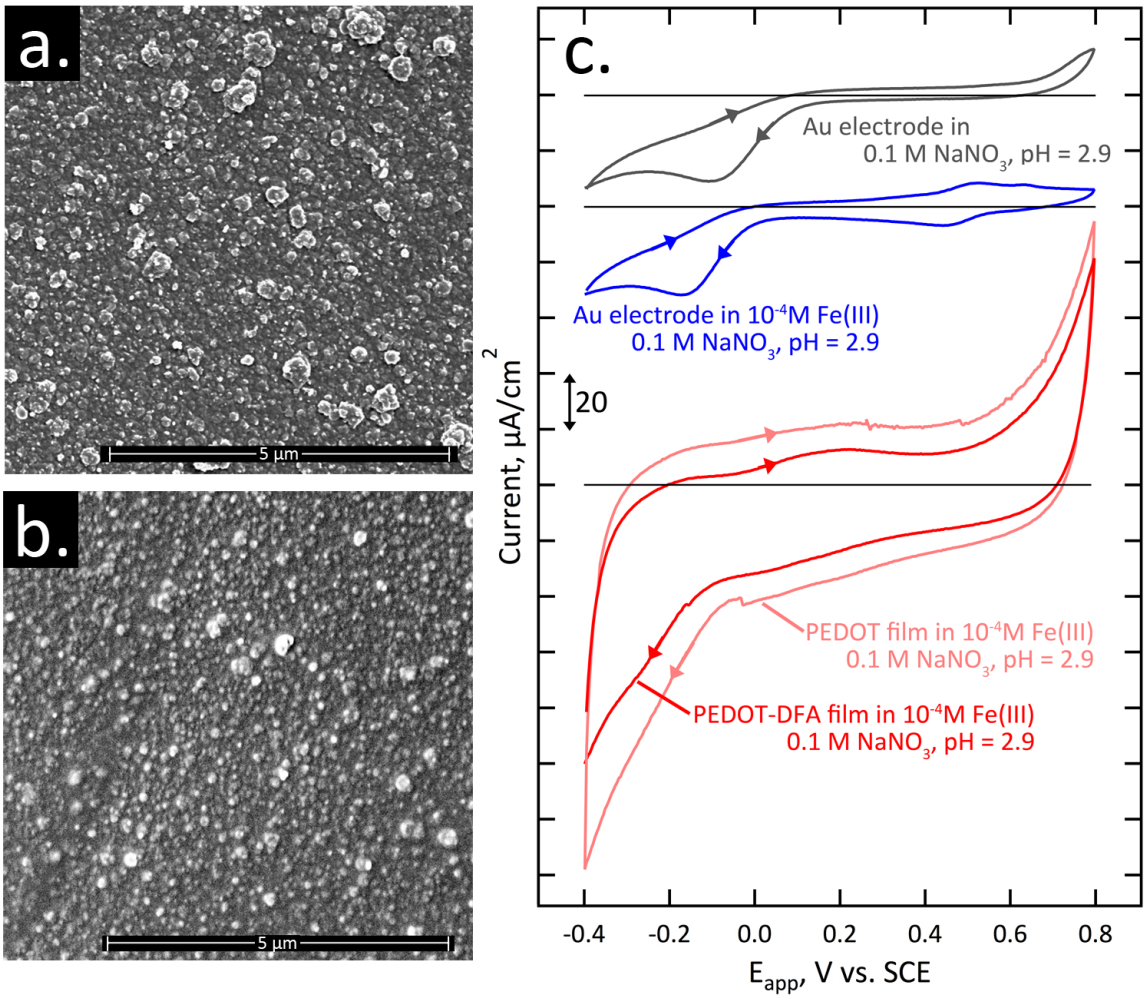

Figure 2.5: SEM images (a,b), and cyclic voltammetry (c) of bare gold electrodes, a PEDOT film and a PEDOT-DFA film. a,b) SEM images of the uncoated surfaces of a PEDOT film (a) and a PEDOT-DFA film (b). c) Cyclic voltammograms for 1.6 mm diameter gold electrodes (top two traces), a PEDOT film (pink trace) and a PEDOT-DFA film (red trace). Scan rate = 20 mV/s for all. The Fe(III)/Fe(II) couple seen at +0.53 vs. SCE at the gold electrode (blue trace) is not seen at either the PEDOT (pink) or the PEDOT-DFA (red) film-covered electrodes.

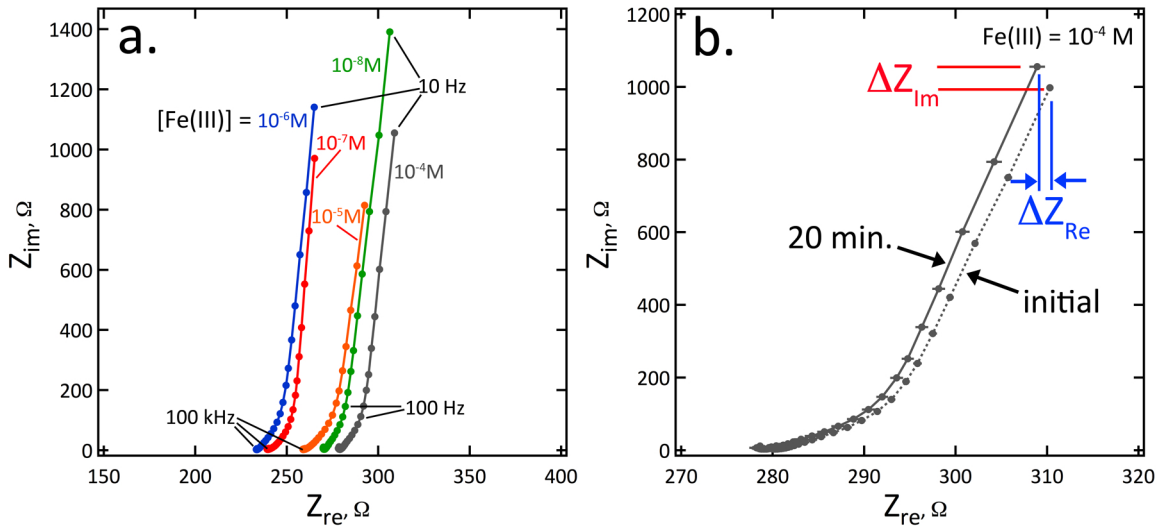

Figure 2.6: Nyquist plots (Z_{Im} *versus* Z_{Re}) for PEDOT/DFA films. a) Five Nyquist plots as a function of Fe(III) concentration, after 20 min. of equilibration in solution. The frequency range from 10 Hz to 100 kHz is shown for each data set. b) Nyquist plots for Fe(III) = 10^{-4} M acquired promptly upon immersion in this solution (dashed line) and after 20 min of equilibration (solid line).

Nyquist plots (Z_{Im} *versus* Z_{Re}) of the EIS data acquired for PEDOT/DFA films equilibrated with Fe(III) (Figure 2.6a) show that Z_{Re} and Z_{Im} are both uncorrelated with Fe(III) concentration over the range from 10^{-8} M to 10^{-4} M. As each of these Nyquist plots were acquired for different PEDOT/DFA films, this result highlights the variability in the impedance properties of PEDOT/DFA films caused, apparently, by uncontrolled variables in the electrodeposition process. However, the influence of this variability can be minimized by comparing the Nyquist plot obtained for films immediately after immersion in the Fe(III) solution, and the same film after 20 min of exposure (Figure 2.6b). Based on the observed impedance shifts, ΔZ_{Re} and ΔZ_{Im} can be defined as, for example, $\Delta Z_{Re} = Z_{Re,eq} - Z_{Re,initial}$. ΔZ_{Re} and ΔZ_{Im} defined in this way allow for the isolation of Fe(III) concentration as a variable in the impedance measurement.

This strategy does not reveal any correlation between ΔZ_{Re} and [Fe(III)] (data not shown), but plots of ΔZ_{Im} versus frequency (Figure 2.7a) show that a correlation between ΔZ_{Im} and [Fe(III)] does exist: The binding of Fe(III) by PEDOT/DFA films causes an increase ΔZ_{Im}

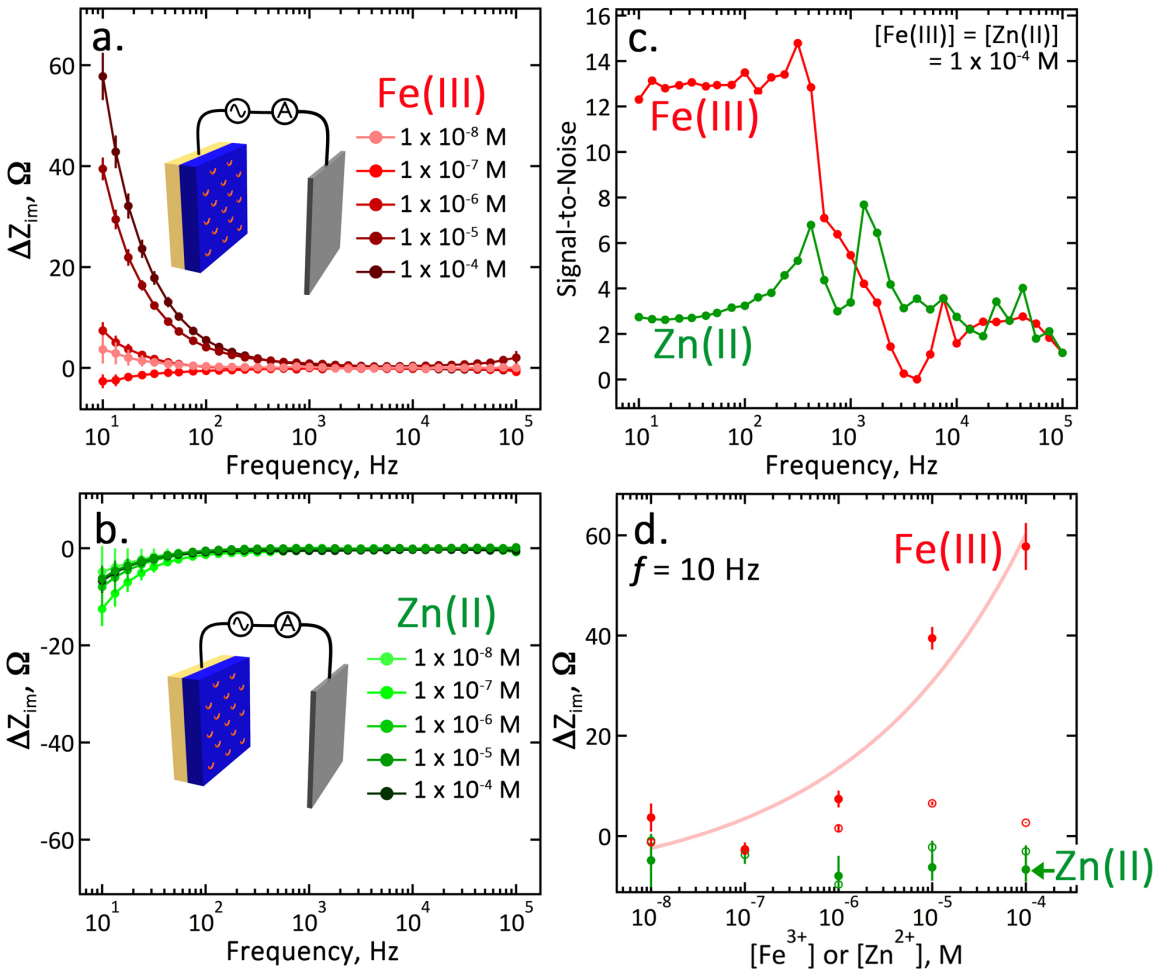

Figure 2.7: Detection of Fe(III) at PEDOT and PEDOT-DFA films on gold electrodes. a,b) Plots of the change in Z_{Im} caused by exposure to Zn(II) or Fe(III), versus frequency for five Fe(III) solutions (a) and five Zn(II) solutions (b). These solutions have metal ion concentrations of 10^{-8} M, 10^{-7} M, 10^{-6} M, 10^{-5} M, and 10^{-4} M. c) Plot of the signal-to-noise ratio (S/N) as a function of frequency for the measurements of Z_{Im} shown in (a) and (b). The noise in this calculation was obtained as the standard deviation of five replicate measurements of Z_{Im} at each frequency. d) Plot of the change in ΔZ_{Im} at $f = 10$ Hz as a function of the concentration of Zn(II) and Fe(III).

by up to 60 Ω at 10 Hz for Fe(III) = 10^{-4} M, and this increase is concentrated at frequencies <100 Hz. (Figure 2.7c) Since $\Delta Z_{Im} = 1/(2\pi fC)$, the positive sign of ΔZ_{Im} indicates that the capacitance of the film decreases as Fe(III) is incorporated. ΔZ_{Im} responds more weakly to Zn(II) (Figure 2.7b) showing a decrease of 4-12 Ω for Zn(II) concentrations spanning the range from 10^{-8} M to 10^{-4} M. This result demonstrates selectivity for the EIS response observed for Fe(III).

The frequency-dependent signal-to-noise (S/N) plot of Fe(III) detection (Figure 2.7c) in the 10^{-4} M solution was obtained by dividing the ΔZ_{Im} by the standard deviation of five consecutive impedance measurements. Defined in this way, the S/N for Fe(III) is fairly constant from 10 Hz to 300 Hz. Above 300 Hz, the S/N drops off sharply as a result of there being little to no signal at higher frequencies (Figure 2.7a). Unfortunately, the signal-to-noise for the measurement of ΔZ_{Im} is just 12-14 at 10 Hz for Fe(III) = 10^{-4} M (Figure 2.7c) and this does not afford the ability to detect Fe(III) below 10^{-5} M (Figure 2.7d). Thus, PEDOT/DFA films are able to detect Fe(III) with some degree of selectivity, but only at relatively high concentrations, above 10^{-5} M.

Detection of Fe(III) by PEDOT-DFA nanowire arrays. Impedance results for PEDOT/DFA films were compared with the measurements of the electrical resistance, R, of arrays of 200 PEDOT/DFA nanowires. Current versus voltage scans at 20 mV/s between -0.50 and +0.50 V at the rest potential for the nanowires were used to measure R as a function of the concentration of Fe(III) (and also Zn(II)). This method of measuring R is tantamount to an EIS measurement of Z_{Re} at an extremely low frequency of ≈0.2 Hz. In the analysis of these data, we plot the change in resistance upon equilibration with the metal ion, ΔR, normalized by the initial resistance, R_0 or $\Delta R/R_0$. $\Delta R/R_0$ is zero for PEDOT nanowires without DFA (Figure 2.8) upon exposure to either in either Zn(II) or Fe(III) up to 10^{-4} M in both ions (Figure 2.8a,c). PEDOT/DFA nanowires also show a nearly undetectable, negative $\Delta R/R_0$

of (-1)-(-2)% for Zn(II) over the range from 10^{-8} M to 10^{-4} M (Figure 2.8b). But a much stronger response is observed to Fe(III) where a negative $\Delta R/R_0$ of up to 34% is observed for 10^{-4} M (Figure 2.8d). The negative value of $\Delta R/R_0$ means that the electrical conductivity of PEDOT/DFA nanowires increases with exposure to Fe(III). Fe(III) at concentrations as low as 10^{-8} M are readily detected as a $\Delta R/R_0$ signal of $\approx$ 5% above a noise floor of 1-2%.(Figure 2.8d). A lower limit-of-detection of 340 pM is calculated using the [Fe(III)] corresponding to $3\sigma_{\Delta R/R_0}$ obtained from regression analysis of the calibration plot shown in Figure 2.8e. Both of these numbers are lower than any so far reported for the detection of Fe(III) by an electrically-based sensor (FET or chemiresistor), to our knowledge (Table 1).

If Fe(III) decreases the resistance of PEDOT/DFA nanowires, why isn't this detected in EIS measurements of PEDOT/DFA films? Simplified equivalent circuits for the PEDOT/DFA system in films and nanowires (Figure 2.9) emphasize the existence of parallel ionic and electronic current paths through this porous conductor. In these schematic diagrams, just the electronic branch of the circuit is directly connected either to the electrode surface or the electrical contacts in the case of nanowires. The ionic branch of the circuit is accessed through the capacitive coupling made available at frequencies, $f > 0$. In both PEDOT/DFA films (Figure 2.9a) and nanowires (Figure 2.9b), the ionic resistance, R_{ionic}, is disposed in parallel with the electronic resistance, R_{elect}. The effective resistance for conductive polymer films, R_{eff}, is approximated by: [1, 2, 43]

$$\frac{1}{R_{eff}} = \frac{1}{R_{ionic}} + \frac{1}{R_{elect}} \tag{2.1}$$

Eq. (1) assumes that Z_{Im} is low enough to provide access to R_{ionic}.

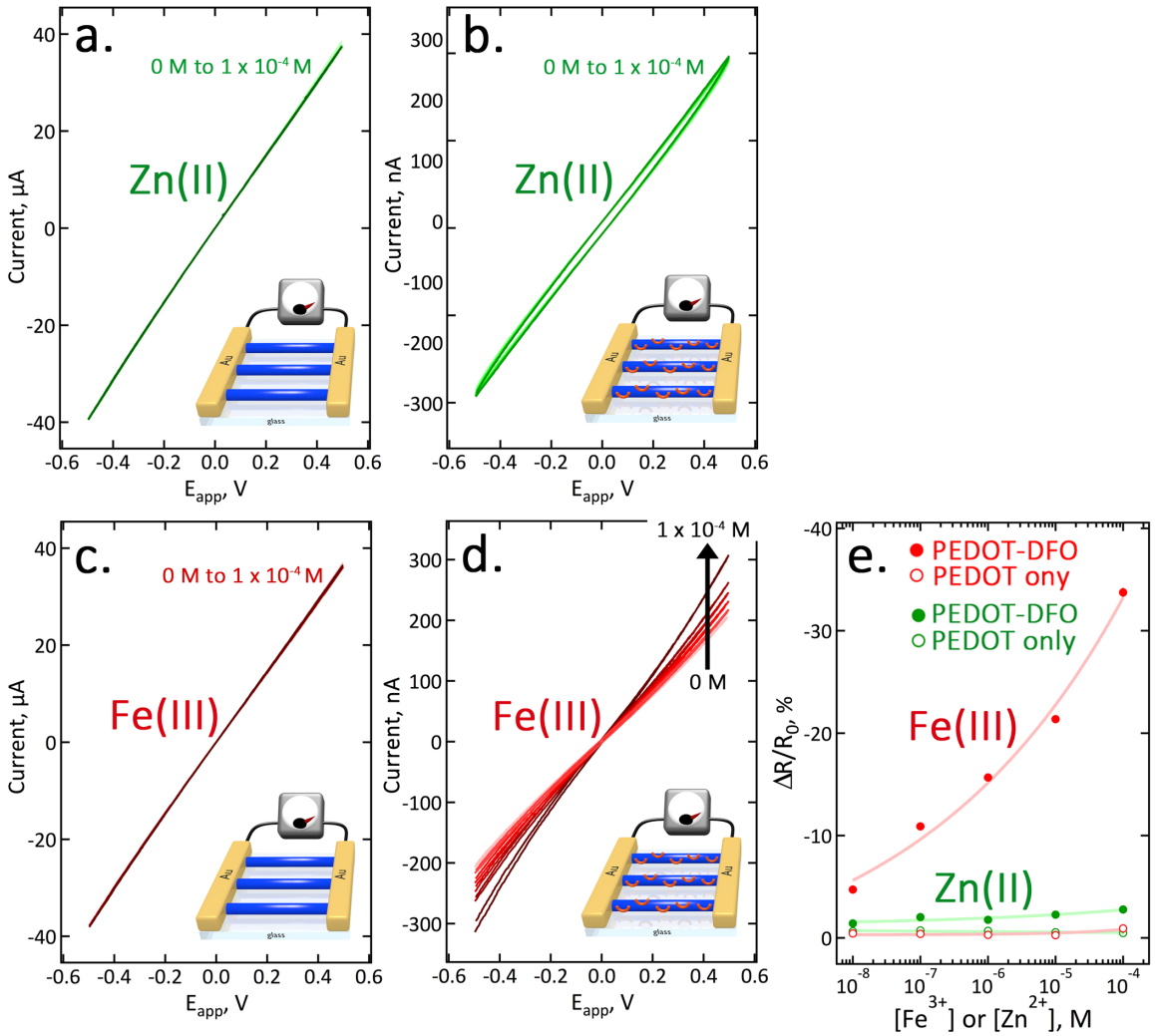

Figure 2.8: Current versus voltage (I-V) curves for PEDOT (a,c) and PEDOT-DFA (b,d) nanowire arrays. a,b) I-V curves acquired in five Zn(II) solutions ([Zn(II)] = 10^{-8} M, 10^{-7} M, 10^{-6} M, 10^{-5} M, and 10^{-4} M) at pure PEDOT nanowires (a) and PEDOT-DFA nanowires (b). All scan rates 20 mV/s. c,d) I-V curves acquired in five Fe(III) solutions ([Fe(III)] = 10^{-8} M, 10^{-7} M, 10^{-6} M, 10^{-5} M, and 10^{-4} M) at pure PEDOT nanowires (c) and PEDOT-DFA nanowires (d). All scan rates 20 mV/s. e) Plot of the change in the measured resistance, R, normalized by the initial resistance, R_0, as a function of [Zn(II)] and [Fe(III)]. Controls (open red circles) are the responses seen for pure PEDOT only nanowires and (open green circles) and the electrical contacts without any nanowires.

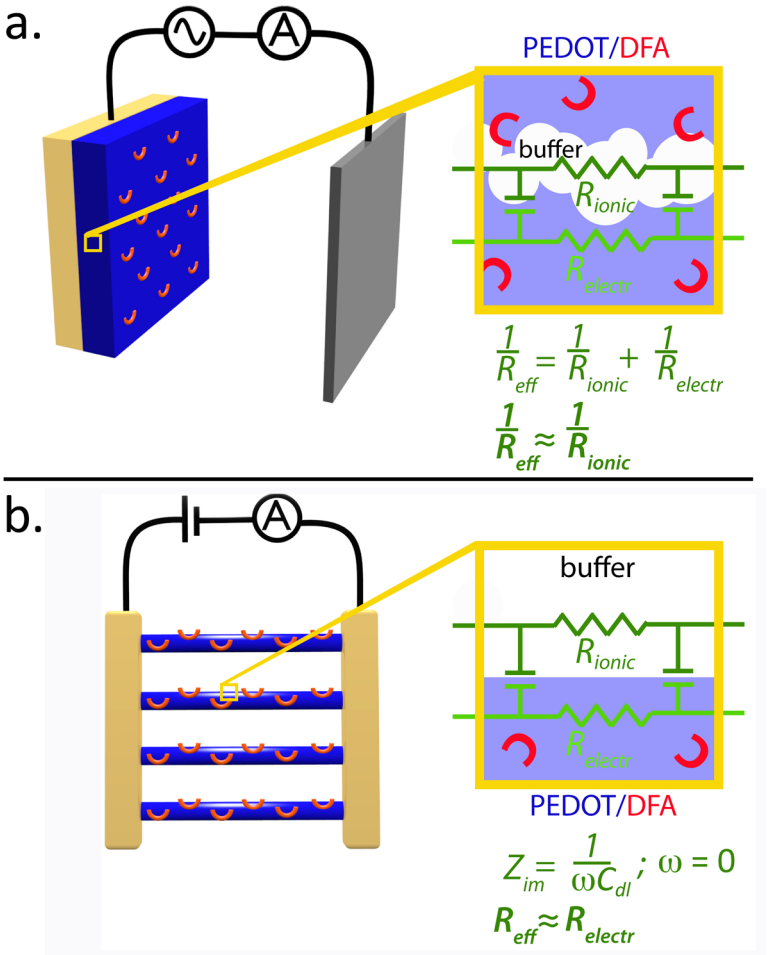

Figure 2.9: Equivalent circuits for an element of a PEDOT/DFA film (a) and PEDOT/DFA nanowire array (b) normal to the direction of current flow. In these schematic diagrams, just the electronic branch of the circuit is directly connected either to the electrode surface or the electrical contacts in the case of nanowires. The ionic branch of the circuit is accessed through the capacitive coupling made available at frequency, f.

Our hypothesis is that the response of PEDOT/DFA to Fe(III) influences primarily R_{elect}; R_{ionic} is unaffected by Fe(III) binding, to first order. This readily explains why PEDOT/DFA nanowires detect Fe(III) binding with high sensitivity: In this case, at $f \approx 0.20$ Hz, $Z_{Im} = 1/(2\pi f C_{dl})$ is large, and the coupling of charge into the electrolyte phase is blocked, affording a direct measurement of R_{elect} between two metal contacts. But PEDOT/DFA films show no resistance response to Fe(III) even at $f = 10$ Hz. This suggests that $R_{elect} >> R_{ionic}$ and that R_{eff} is dominated by R_{ionic} across the entire frequency range we have explored - from 100 kHz to 10 Hz. In fact, we see from the Nyquist plots of Figure 2.6a that the dispersion of R_{eff} over this entire frequency range is just 50 Ω. This scenario requires that R_{electr} is relatively large for the PEDOT/DFA. Our nanowire measurements provide a direct opportunity to measure this for PEDOT/DFA nanowires that have not been exposed to Fe(III). These measurements show that individual PEDOT/DFA nanowires with dimensions of 710 nm × 50 nm × 25 μm have a $R = 480 \pm 10$ MΩ. This translates into a resistivity, $\rho = 68$ Ω cm, or a conductivity of just 0.015 S/cm - approximately a factor of 50 - 5000 lower than is typically measured for PEDOT-PSS films (0.80 - 80 S/cm) [22, 24].

2.5 Conclusions

We describe the preparation and properties of DFA-doped PEDOT films and nanowires for the detection of Fe(III) in high ionic-strength aqueous solutions. An array of ≈200 PEDOT/DFA nanowires are far superior for this purpose, relative to a film, enabling the detection of Fe(III) across the range from [Fe(III)] = 10^{-8}M to 10^{-4}M. Based upon the signal-to-noise of this measurement, a limit-of-detection is estimated to be 340 pM. The sensitivity of these nanowire arrays for Fe(III) is superior to that provided by ISEs and all other electrical based sensors including chemFETs and other types of chemiresistors, to ow

knowledge (Table 1). Remarkably, this method is also label-free and it does not require the use of an added redox couple.

These doped-PEDOT nanowire arrays are easily prepared by electrodeposition using the LPNE method, and the incorporation of the DFA chelator requires no additional processing steps, as it is directly added to the polymerization solution. In principle, this paradigm could be generalizable for other ions, using other molecular chelators.

Table 2.1: Nanowire-Based Chemiresistors and Transistors for the Detection of Metal Ions

Nanowire Description	Ionophore	Detected Metal Ions	Conc. Range	$LOD_{M^{n+}}$	Ref
Semiconductor					
silicon FET	calmodulin	Ca^{2+}	25 μM only	$\approx$5 μM (est.)	[14]
silicon FET	tripeptide	Cu^{2+}	1.0 - 1 nM	1 nM (est.)	[10]
silicon FET	oligopeptide	Cu^{2+}, Pb^{2+}	n.a.	1 nM (Cu^{2+})	
				10 nM (Pb^{2+})	[11]
silicon FET	3-(mercaptopropyl)	Cd^{2+}, Hg^{2+}	10^{-2}-10^{-4} M (Hg^{2+})	10 mM (Hg^{2+})	
	triethoxysilane		10^{-3}-10^{-7} M (Cd^{2+})	0.10 μM (Cd^{2+})	[31]
carbon SWNT FET	PANI/oligopeptide	Cu^{2+}	10^{-6}-10^{-10} M (Cu^{2+})	1 pM (Cu^{2+})	
	PPy/oligopeptide	Ni^{2+}	10^{-6}-10^{-10} M (Ni^{2+})	60 pM (Ni^{2+})	[19]
rGO FET	calmodulin	Ca^{2+}, Hg^{2+}	10^{-6}-10^{-4} M (Ca^{2+})	1 μM (Cu^{2+})	
			10^{-9}-10^{-11} M (Hg^{2+})	1 nM (Ni^{2+})	[50]
Polymer					
PPy CR	NTA	Cu^{2+}	10^{-14} M - 0.10 nM	0.01 pM	[4]
PPy CR	tripeptide	Cu^{2+}	10^{-3} - 20 nM	20 nM	[28]
PEDOT CR	**DFA**	**Fe^{3+}**	**10^{-4} M - 10 nM**	**10 nM (meas.)**	
				0.3 nM (calc.)	**this work**

[a]Abbreviations: FET - field effect transistor, CR - chemiresistor, PPy - poly(pyrrole), PANI - poly(aniline), rGO - reduced graphene oxide, PEDOT - poly(3,4-ethylenedioxythiophene), NTA -nitrilotriacetic acid,DFA - deferoxamine, $LOD_{M^{n+}}$ - limit-of-detection.
[b]Measured response was attributed to both anion and cation.

Chapter 3

Glucose Detection

3.1 Abstract

This chapter explores the work in creating a non-enzymatic impedance-based glucose sensor. An alternative biological recognition layer of 3-thienylboronic acid (3TBA) was incorporated into a electropolymerized thiophene (Th) film. This research, using a 3 electrode cell set-up as described in chapter 1, protein detection , was a novel concept and began by developing a method to incorporate 3TBA into a polymer film. Incorporation was verified using x-ray photoelectron spectroscopy (XPS) and electrochemical impedance spectroscopy (EIS) was used to measure fructose. Further optimization is required to determine if 3TBA-Th films or nano structures can be used as an alternative to traditional glucose monitoring.

3.2 Introduction

The 2015 IDF Diabetes Atlas, from the International Diabetes Foundation, estimated that 415 million people worldwide have diabetes [53]. There are three types: type 1 (or juvenile),

type 2 (or adult onset), and gestational. Type 1 diabetes is caused by an autoimmune reaction in which the body's defense system attacks the insulin-producing beta cells in the pancreas. A person with type 1 diabetes needs insulin injections everyday to live, and this form of diabetes is currently incurable [53]. Type 2, the most common form, is from having excess body weight, low physical activity, and poor nutrition, causing the body to become resistant to insulin. The treatment is to change life habits and sometimes oral medications are prescribed. Gestational diabetes occurs during pregnancy and can also be treated by changing life habits and sometimes oral medications.

Some of the long term complications related to diabetes are kidney failure, blindness, cardiac problems, circulation problems, and loss of feeling in areas used for glucose monitoring. These issues lead to loss of productivity and the long-term support needed to overcome these complications place a large financial burden on individuals, their families, and the health system. The majority of countries spend between 5% and 20% of their total health expenditure on diabetes, this equals approximately $320 billion for the U.S. alone [53]. For point-of-care purposes, continuous glucose monitoring (CGM) devices are considered the best method for diabetes management [13].

Glucose (or α-D-glucopyranose) is a monosaccharide with the formula $C_6H_{12}O_6$ and is used by organisms for energy [8].Other saccharides, including galactose and fructose, have the same formula as glucose, $C_6H_{12}O_6$, and show no structural difference except configurations of certain stereocentres, as shown in Figure 3.1 [58].

Commercially available glucose meters use the glucose oxidase (GOx) enzyme to detect glucose in the blood. GOx catalyzes the oxidation of glucose to produce gluconic acid as shown in the following equation:

$$\mathrm{D{-}glucose} + O_2 + H_2O \xrightarrow{\mathrm{GOx}} \mathrm{D{-}gluconic\ acid} + H_2O_2$$

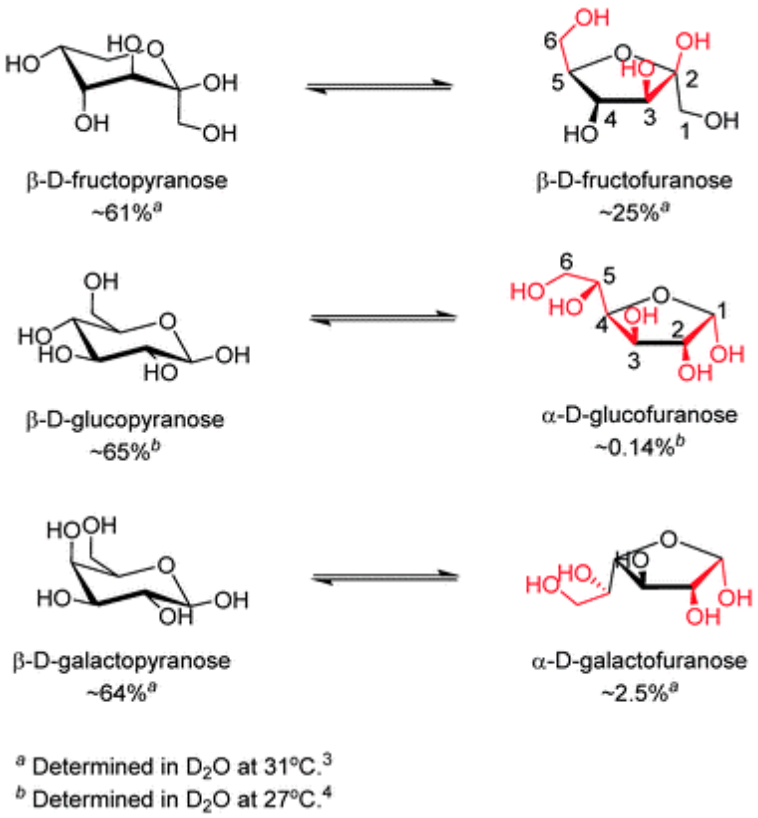

Figure 3.1: Equilibria between the dominant form (left) and the form that contains a syn-periplanar anomeric hydroxyl pair (right) of D-fructose (top), D-glucose (middle) and D-galactose (bottom). Potential boronic acid binding sites are highlighted in red. Positions for hydroxyl groups are numbered in β-D-fructofuranose and α-D-glucofuranose [58].

This enzyme was first used to measure glucose concentration in biological fluids in 1967 [37, 54, 42]. Since then, some improvements have been made but GOx is still susceptible to a variety of environmental factors. This reaction is a function of humidity, both high and low humidity, and can be significantly harmful to the sensors during use as well as in storage [37]. Enzyme activity is affected by temperatures above 40 °C, pH below 2 and above 8, and toxic chemicals [42, 45]. Reproduciblity is also a critical issue in quality control due to possible thermal and chemical deformation of GOx during fabrication, storage or use [37].

Continuous glucose monitoring devices work by collecting a small amount of blood and measuring the serum glucose level, allowing diabetics to adjust eating habits and/or insulin injections. These devices can be categorized as extremely invasive, minimally invasive, and noninvasive depending on whether the CGM device penetrates/breaks the skin and/or the sample, at a particular point in time, is measured extracorporeally [55]. Current monitors are considered minimally invasive and are used by pricking the skin with a lancing device to draw a small amount of blood that is then placed on to a test strip. It is recommended that a diabetic monitor their blood glucose levels 4-5 times a day, resulting in almost 1800 times annually [63]. The American Diabetes Association indicates the target range for serum glucose levels, dependent on before or after a meal, for most non-pregnant adults with diabetes to be between 80–180 mg/dL [3], which is equal to 4.4–10 mM.

The susceptibilities and invasiveness of enzymatic glucose sensors have encouraged many researchers to develop electrochemical glucose sensors that do not require the use of enzymes or blood serum samples. One possible non-enzymatic alternative is boron acids (boric, boronic and borinic) [37]. The reversible covalent interaction of boronic acids with cis-1,2- or 1,3-diols to form five- or six-membered cyclic esters, respectively, has proven sufficiently strong, enabling binding of saccharides at mM or sub-mM levels, rendering boronic-acid based saccharide sensing in biologically relevant scenarios possible [58]. The depiction of

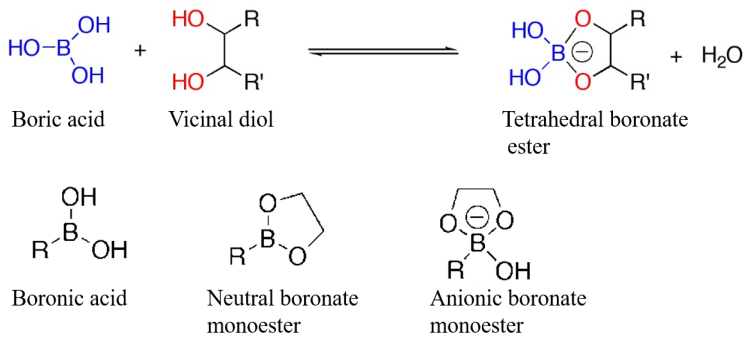

Figure 3.2: Boric acid interactions with vicinal diol of sugar, top reaction. Boronic acid and possible esters with ethylene glycol, bottom scheme [36].

boronic acid interaction with vicinal diols of saccharides (like glucose and fructose) was created by Pappin et al. [36] and is shown in Figure 3.2.

The relative affinity of boronates for diols in most carbohydrates is of the order: cis-1,2-diol > 1,3-diol >> trans-1,2-diol, meaning certain monosaccharides have an intrinsically higher affinity for boron acids [36]. Lorand and Edwards published work quantifying the affinity of boric and phenylboronic acids for simple diols (e.g. ethylene glycol, catechol) and common monosaccharides (i.e. glucose, fructose, mannose, galactose) in 1959 [36, 30]. To our knowledge, there is no literature defining the binding constant of 3-thienylboronic acid (3TBA) to glucose or fructose, however the binding constant of phenylboronic acid with fructose is 4370 M^{-1} while that with glucose is 110 M^{-1} [58]. It is also of significance to note from Figure 3.2 that upon binding to saccharides a negatively charged boronate ester forms at high pH, thus a positive charge, such as that from ammonium or pyridinium cation, may be incorporated into the structure of the sensor to facilitate the boronic acid–saccharide interaction [58]. Also, selectivity requires properly positioned and structurally rigid diboronic acids, which can be addressed with the construction of multiboronic acid scaffolds.

Successful sensors have been made using boronic acids, for example Lerner et al. made carbon nanotube transistors functionalized with pyrene-1-boronic acid. This sensor responds to glucose in the range 1 μM–100 mM, which includes typical glucose concentrations in human

blood and saliva [26]. Shen et al. produced boronic acid functionalized carbon dots for fluorescent blood sugar sensing in the range of 9–900 μM [46].

This chapter proposes the use of 3TBA as a recognition layer for the detection of fructose and in the future glucose. Methods for polymerizing thiophene compounds, such as poly(3,4-ethylenedioxythiophene), PEDOT, mentioned in previous chapters, have been developed and were modified to polymerize 3TBA. Fabrication processes and steps performed using a three electrode set-up, as mentioned in chapter 1, were used first to verify a 3TBA containing film could be made. To verify the presence and binding capabilities of 3TBA X-ray photoelectron spectroscopy (XPS) and electrochemical impedance spectroscopy (EIS) were used. Preliminary experiments using 50 mM of fructose show 3TBA has the potential to become a non-enzymatic electochemical biosensor.

3.3 Experimental

Chemicals and Materials – All chemicals were ordered from Sigma Aldrich and used as received unless otherwise specified; 3,4-ethylenedioxythiophene (EDOT, 97%), lithium perchlorate (99.99%, trace metals basis), glucose, fructose, thiophene (Th), 3-thienylboronic acid (3TBA, 95%), and sulfuric acid (99.999%). Phosphate buffered saline (PBS 1X, pH 7.4), filter-sterilized through a 0.22 m pore size membrane (Corning), was used as the run buffer and for analyte sample preparation. Water for all solutions and rinse steps was processed by a Millipore Milli-Q UV system (resistance >18 MΩ cm). Electrochemical polymerization experiments were conducted in 12.5 mM $LiClO_4$ in ultrapure dry acetonitrile (ACN), obtained by filtering reagent grade ACN using a Jorg Meyer Phoenix SDS column purification system.

Synthesis of TBA-TP films – Circular gold or platinum electrodes (1.6 mm diameter, BASi Inc.) were manually polished using a polishing microcloth (Buehler) in conjunction with diamond polishing pastes of decreasing particle sizes, beginning with 1 μm and proceeding to 0.5 μm and 0.25 μm (Ted Pella). Polished electrodes were then cleaned by sonication in Milli-Q water for 10 min and dried with a lab airgun. A flame-annealed platinum foil counter electrode was wrapped around the polymer barrel of the polished circular electrode, as described in previous chapters. These electrodes were then placed in the 3TBA-Th plating solution (variable concentrations of 3TBA, 0.5 mM Th, 12.5 mM $LiClO_4$ in dry ACN). Electropolymerization occurred by cycling between 0 and 1.8 V vs. SCE for 10 cycles at a scan rate of 20 mV/s. Synthesized films were rinsed in Milli-Q water and immediately transferred into PBS solution.

Electrochemical Impedance Spectroscopy Analysis – All EIS measurements are made using a PARSTAT 2273 potentiostat controlled by POWERSine software (Princeton Applied Research, Oak Ridge, TN). Five consecutive EIS measurements are acquired at a 10 mV voltage modulation amplitude, over 50 data points, spanning 0.1 Hz to 1 MHz, at 0 V versus open circuit.

X-ray Photoelectron Spectroscopy – XPS measurements were performed with an ESCALAB MKII (VG Scientific) surface analysis instrument as by M. Le et al. [25].

3.4 Results and Discussion

First attempts to incorporate 3TBA were to electropolymerize 3TBA in the presence of EDOT using the same parameters as described in previous chapters, in aqueous solution. Using an aqueous EDOT solution for polymerization is much easier than using an organic solvent, like ACN, because organic solvents need to be dried using special equipment. How-

ever organic solutions can polymerize chemicals at greater potentials; in aqueous solutions hydrogen evolution and oxygen reduction occur outside 1.2 V.

Films electrochemically polymerized using an aqueous solution were grown, however 3TBA incorporation could not be verified. It is believed that the low solubility of 3TBA in aqueous solution prevented it from being polymerized into the PEDOT film. No data for 3TBA-PEDOT films are shown. The next experiments performed used procedures polymerizing Th by Tanaka et al. [52] to electropolymerize 3TBA in dry ACN. These experiments provided light films that easily washed or brushed off the gold electrode and no data is shown. Lastly, variable concentrations of Th were mixed into 3TBA in dry ACN creating 3TBA-Th films. These films were successfully polymerized on platinum electrodes, as there were adhesion problems with gold electrodes. The 3TBA-Th films easily washed or wiped off the gold disk electrodes and did not grow on physically vapor deposited (PVD) gold electrodes(fabrication for PVD electrodes is discussed in previous chapters). After electropolymerization on PVD gold electrodes, the electrode was eroded off and no film was formed. The polymerization cycles of films grown on Pt electrodes are shown in Figure 3.3. This figure shows the comparison of two films: a. 3TBA-Th (1 mM 3TBA to 0.5 mM Th) and b. Th (1.5 mM). All parameters are identical for these two electropolymerizations, but as shown the 3TBA-Th film polymerization was hindered by the incorporation of 3TBA. Further studies into the mechanics of how 3TBA polymerizes are needed in order to understand why the polymerization is hindered, but are not investigated or discussed in this research.

Characterization and sensing abilities of 3TBA-Th films – Experiments were performed to determine the minimal concentration of pure Th needed to form a dark, dense film. Dark films are indicators of dense film growth which theoretically provide well covered metal electrode, maximum diol binding sites from 3TBA, and film stability. The lowest concentration ratio to produce 3TBA-Th films was determined to be 0.1 M 3TBA to 0.05 M Th (2:1 ratio films). To verify incorporation of 3TBA into 3TBA-Th films, XPS was performed on three

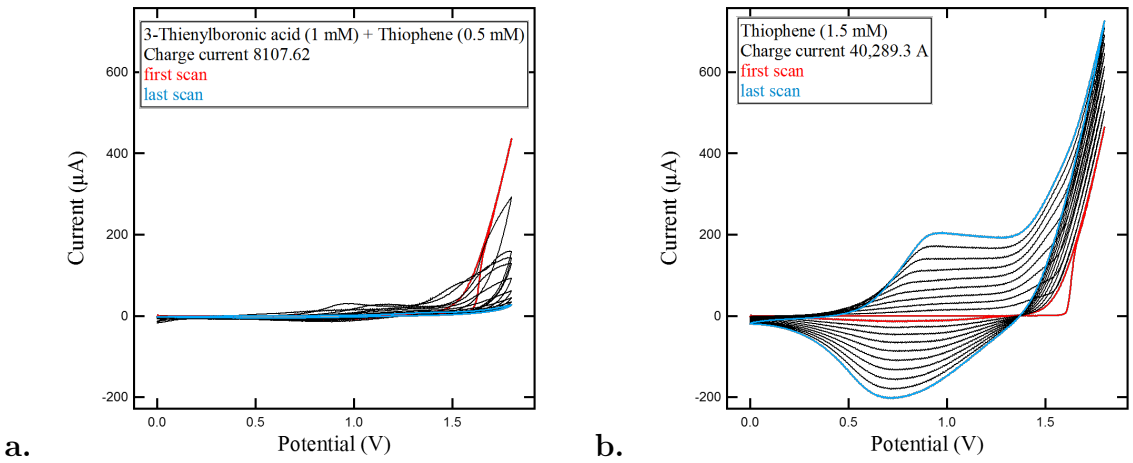

Figure 3.3: a. 3TBA-Th film growth. b. Th film growth. Charge current shows the two films do not grow the same.

films of varying 3TBA:Th ratio, 0:1 in black, 1:1 in red, and 2:1 in green, are shown in Figure 3.4. The increase of the B1s signal peaks as 3TBA concentration ratio increases verifies 3TBA incorporation into the films.

Fructose was used as the target analyte instead of glucose in order to ensure the maximum amount of binding occurs, as stated above fructose has a much higher binding constant to boronic acids than glucose. In future experiments, after these films are verified and optimized, glucose can be used as the target analyte.

Experiments were performed on fresh films for each data set. After electropolymerization the film was submerged in 20 mL of PBS and then left to equilibrate for 2 hours. Once stable, 1 mL was removed from the 20 mL total volume and fresh PBS was added, this was done 3 times, a 20 minute wait time between injection and EIS measurement, to verify minimal signal change from solution disturbances. Lastly, 1 mL was removed then 1 ml of fructose solution was added to make the total solution concentration equal to 50 mM fructose, 20 minute exposure time then EIS measurement was taken.

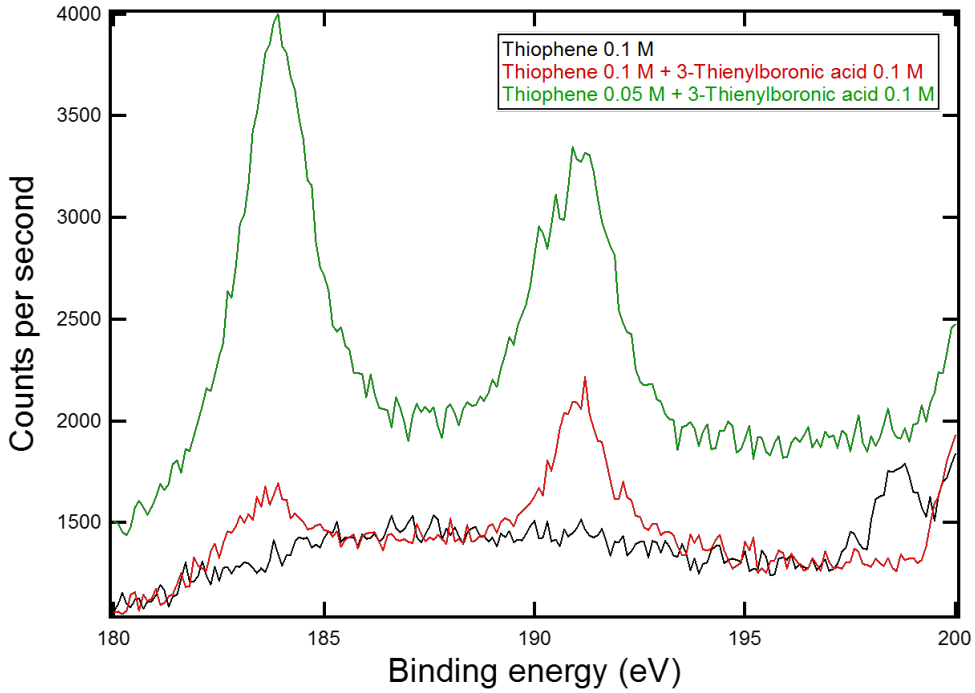

Figure 3.4: XPS data for three films, TBA-Th 0:1, 1:1 TBA-Th, 2:1 TBA-Th, showing the increase for B1s signal peaks as the 3TBA concentration is increased.

EIS data is provided as normalized data vs. frequency plots in Figure 3.5. As described in previous chapters, normalized data is expressed as,

$$\frac{\Delta Z_m}{Z_0}$$

where Z_0 is the initial impedance taken in PBS, and ΔZ_m is Z_m-Z_0, where Z_m is the impedance taken after the initial impedance. Figure 3.5 shows data for a 3TBA-Th film (in red) and a Th only film (in gold). It was verified that PBS–only exposures (shown in black and grey) had minimal signal change especially in the 1,000 to 10,000 Hz range for both Z_{re} and Z_{img}. The 3TBA-Th film (in red) has a Z_{img} signal change at just after 1,000 Hz to and drops off just before 1 MHz. There is a similar trend in the Th-only film (in gold) but it is decreased and might be attributed to solution change. To properly compare the signal change from fructose the normalized data for Z_{re} and Z_{img} from the 3TBA-Th and Th-only films are

overlaid and shown in Figure 3.6. This figure clearly shows the fructose signal change in the Z_{img} data.

3.5 Conclusions

The experiments here show 3TBA was incorporated into a film that it can be used to detect fructose. Thiophene, Th, proved to be an acceptable interface, providing minimal signal change when exposed to fructose. However, this research is far from replacing the current CGM devices that are now commercially available. It would be desirable, as mentioned in chapter 1, to remove the necessity of the reference (RE) and counter electrodes (CE). By removing these elements the sensor will become less expensive (removal of CE), more reproducible (removal of RE), and have a longer storage life (removal of RE). Attempts to further this research and progress into a smaller, more effective sensor were halted by the obstacles of needing an organic polymerization solution. Optimization methods used in previous chapters are unavailable because these steps require an aqueous polymerization solution due to the use of photoresist. 3TBA deposition requires an organic polymerization solution which will dissolve the photoresist. Future investigation into selectivity is needed; experiments using glucose and determining the difference in signal between fructose and glucose were not performed. Synthesis of a multiboronic compound as discussed in the introduction is required to improve the selectivity for glucose. Also, the ability of boronic acids to reversibly bind sugars was not investigated, but this ability has the potential to make a 3TBA-Th sensor reusable. Unfortunately many questions about the abilities of 3TBA as a glucose sensor are unanswered, but is was shown that 3TBA has great potential to become an alternative to traditional GOx devices.

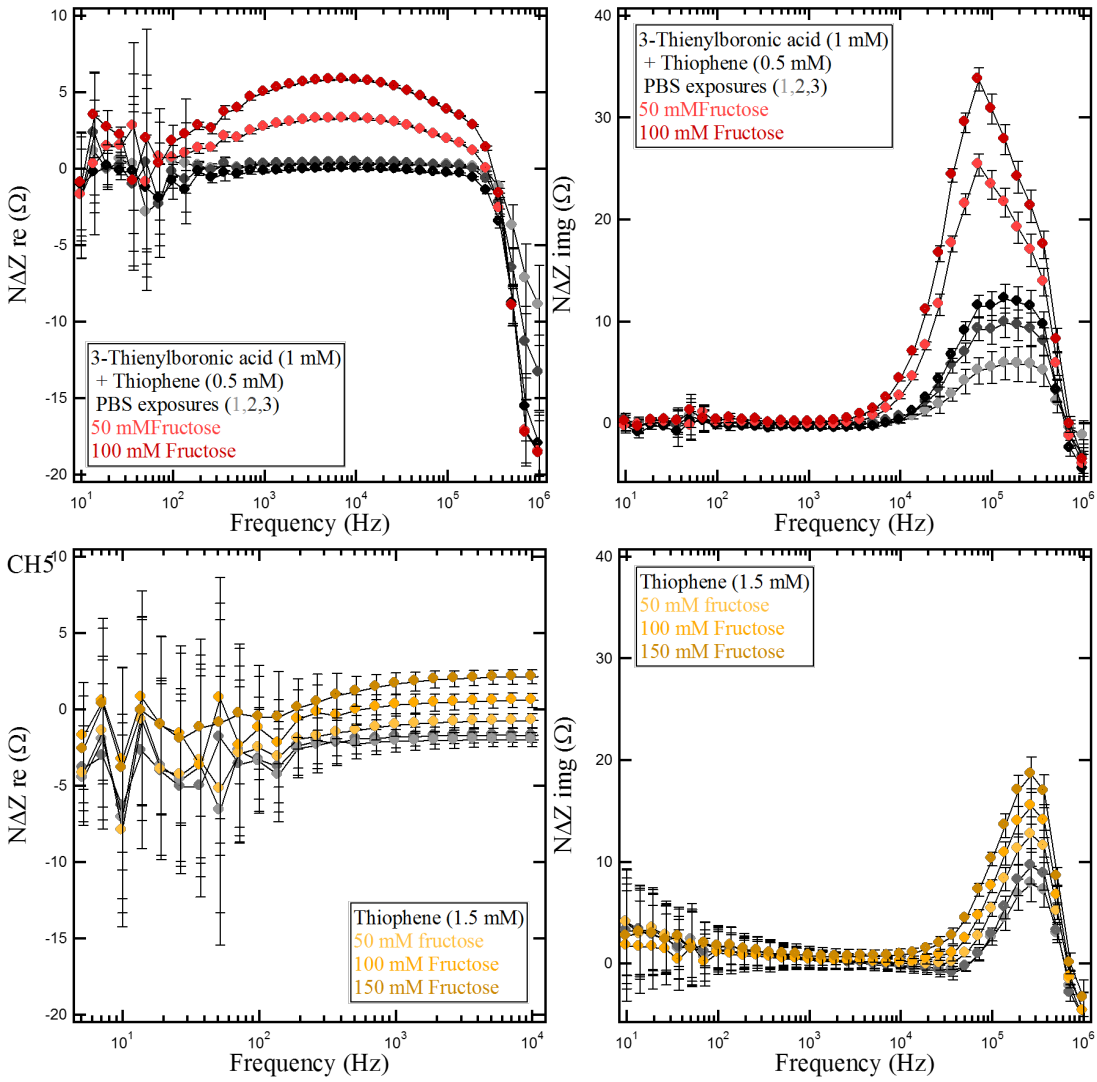

Figure 3.5: Normalized data of fructose addition for 3TBA-Th film in red and Th only film in yellow.

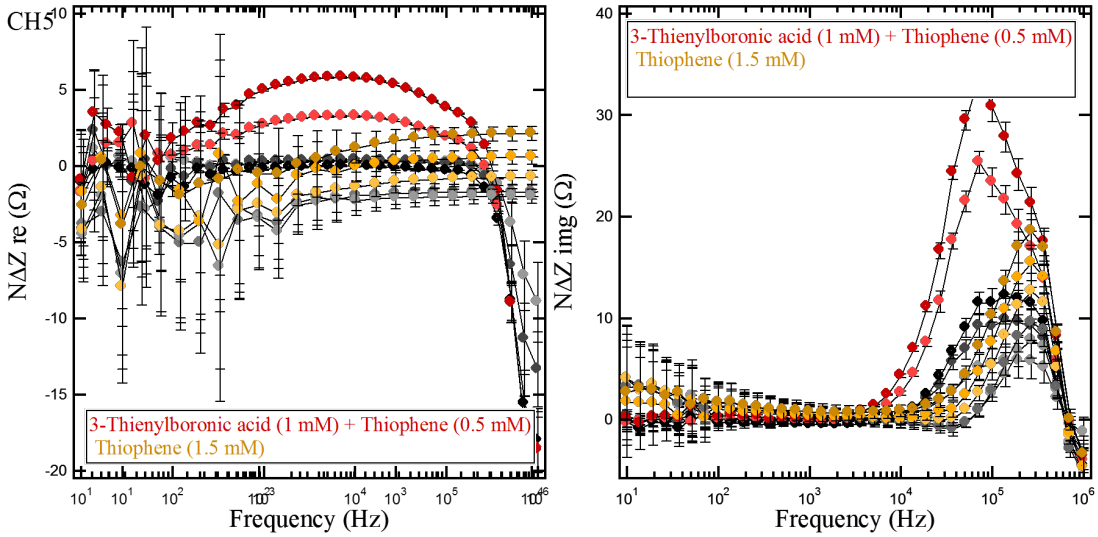

Figure 3.6: EIS Normalized data overlay of fructose addition for 3TBA-Th film (red) and Th–only film (yellow).

Bibliography

[1] W. J. Albery, C. M. Elliott, and A. R. Mount. A transmission line model for modified electrodes and thin layer cells. *J. Electroanal. Chem. interfacial Electrochem.*, 288(1):15–34, 1990.

[2] W. J. Albery and A. R. Mount. A second transmission line model for conducting polymers. *J. Electroanal. Chem. interfacial Electrochem.*, 305(1):3–18, 1991.

[3] American Diabetes Association. Checking Your Blood Glucose, 2017.

[4] C. L. Aravinda, S. Cosnier, W. Chen, N. V. Myung, and A. Mulchandani. Label-free detection of cupric ions and histidine-tagged proteins using single poly (pyrrole)-NTA chelator conducting polymer nanotube chemiresistive sensor. *Biosens. Bioelectron.*, 24(5):1451–1455, 2009.

[5] M. A. Arnold and M. E. Meyerhoff. Ion-selective electrodes. *Anal. Chem.*, 56(5):20R—-48R, 1984.

[6] J. A. Arter, J. E. Diaz, K. C. Donavan, T. Yuan, R. M. Penner, and G. A. Weiss. Virus–polymer hybrid nanowires tailored to detect prostate-specific membrane antigen. *Anal. Chem.*, 84(6):2776–2783, 2012.

[7] J. A. Arter, D. K. Taggart, T. M. McIntire, R. M. Penner, and G. A. Weiss. Virus-PEDOT nanowires for biosensing. *Nano Lett.*, 10(12):4858–4862, 2010.

[8] C. Batema. What Is the Function of Monosaccharide in Biology? — Education - Seattle PI, 2017.

[9] M. L. Beckett, L. H. Cazares, A. Vlahou, P. F. Schellhammer, and G. L. Wright. Prostate-specific membrane antigen levels in sera from healthy men and patients with benign prostate hyperplasia or prostate cancer. *Clin. cancer Res.*, 5(12):4034–40, dec 1999.

[10] X. Bi, A. Agarwal, N. Balasubramanian, and K.-L. Yang. Tripeptide-modified silicon nanowire based field-effect transistors as real-time copper ion sensors. *Electrochem. commun.*, 10(12):1868–1871, 2008.

[11] X. Bi, A. Agarwal, and K.-L. Yang. Oligopeptide-modified silicon nanowire arrays as multichannel metal ion sensors. *Biosens. Bioelectron.*, 24(11):3248–3251, 2009.

[12] J. P. Chambers, B. P. Arulanandam, L. L. Matta, A. Weis, and J. J. Valdes. Biosensor recognition elements. *Curr. Issues Mol. Biol.*, 10(1):1–12, jan 2008.

[13] C. Chen, X.-L. Zhao, Z.-H. Li, Z.-G. Zhu, S.-H. Qian, and A. Flewitt. Current and Emerging Technology for Continuous Glucose Monitoring. *Sensors*, 17(1):182, jan 2017.

[14] Y. Cui, Q. Wei, H. Park, and C. M. Lieber. Nanowire nanosensors for highly sensitive and selective detection of biological and chemical species. *Science (80-.).*, 293(5533):1289–1292, 2001.

[15] A. Deronzier and J. C. Moutet. Functionalized polypyrroles. New molecular materials for electrocatalysis and related applications. *Acc. Chem. Res.*, 22(7):249–255, 1989.

[16] A. F. Diaz, K. K. Kanazawa, and G. P. Gardini. Electrochemical polymerization of pyrrole. *J. Chem. Soc. Chem. Commun.*, (14):635–636, 1979.

[17] K. C. Donavan, J. A. Arter, R. Pilolli, N. Cioffi, G. A. Weiss, and R. M. Penner. Phage encapsulated Poly (3, 4-ethylenedioxythiophene)(PEDOT) film biosensors. In *Abstr. Pap. Am. Chem. Soc.*, volume 241. AMER CHEMICAL SOC 1155 16TH ST, NW, WASHINGTON, DC 20036 USA, 2011.

[18] K. C. Donavan, J. A. Arter, R. Pilolli, N. Cioffi, G. A. Weiss, and R. M. Penner. Virus-Poly (3, 4-ethylenedioxythiophene) Composite Films for Impedance-Based Biosensing. *Anal. Chem.*, 83(7):2420–2424, 2011.

[19] E. S. Forzani, X. Li, P. Zhang, N. Tao, R. Zhang, I. Amlani, R. Tsui, and L. A. Nagahara. Tuning the Chemical Selectivity of SWNT-FETs for Detection of Heavy-Metal Ions. *Small*, 2(11):1283–1291, 2006.

[20] V. K. Gupta, A. K. Jain, S. Agarwal, and G. Maheshwari. An iron (III) ion-selective sensor based on a μ-bis (tridentate) ligand. *Talanta*, 71(5):1964–1968, 2007.

[21] C. M. Hangarter, M. Bangar, A. Mulchandani, and N. V. Myung. Conducting polymer nanowires for chemiresistive and FET-based bio/chemical sensors. *J. Mater. Chem.*, 20(16):3131–3140, 2010.

[22] S. K. M. Jönsson, J. Birgerson, X. Crispin, G. Greczynski, W. Osikowicz, A. W. D. Van Der Gon, W. R. Salaneck, and M. Fahlman. The effects of solvents on the morphology and sheet resistance in poly (3, 4-ethylenedioxythiophene)–polystyrenesulfonic acid (PEDOT–PSS) films. *Synth. Met.*, 139(1):1–10, 2003.

[23] K. Kaneto, K. Yoshino, and Y. Inuishi. Electrical properties of conducting polymer, poly-thiophene, prepared by electrochemical polymerization. *Jpn. J. Appl. Phys.*, 21(9A):L567, 1982.

[24] J. Y. Kim, J. H. Jung, D. E. Lee, and J. Joo. Enhancement of electrical conductivity of poly (3, 4-ethylenedioxythiophene)/poly (4-styrenesulfonate) by a change of solvents. *Synth. Met.*, 126(2):311–316, 2002.

[25] M. Le, Y. Liu, H. Wang, R. K. Dutta, W. Yan, J. C. Hemminger, R. Q. Wu, and R. M. Penner. In Situ Electrical Conductivity of Li_xMnO_2 Nanowires as a Function of x and Size. *Chem. Mater.*, 27(9):3494–3504, may 2015.

[26] M. B. Lerner, N. Kybert, R. Mendoza, R. Villechenon, M. A. Bonilla Lopez, and A. T. C. Johnson. Scalable, non-invasive glucose sensor based on boronic acid functionalized carbon nanotube transistors. *Cit. Appl. Phys. Lett*, 102(183113), 2013.

[27] M. Lin, M. Cho, W.-S. Choe, Y. Son, and Y. Lee. Electrochemical detection of copper ion using a modified copolythiophene electrode. *Electrochim. Acta*, 54(27):7012–7017, 2009.

[28] M. Lin, M. Cho, W.-S. Choe, J.-B. Yoo, and Y. Lee. Polypyrrole nanowire modified with Gly-Gly-His tripeptide for electrochemical detection of copper ion. *Biosens. Bioelectron.*, 26(2):940–945, 2010.

[29] M. Lin, M. S. Cho, W. S. Choe, and Y. Lee. Electrochemical analysis of copper ion using a Gly–Gly–His tripeptide modified poly (3-thiopheneacetic acid) biosensor. *Biosens. Bioelectron.*, 25(1):28–33, 2009.

[30] J. P. Lorand and J. O. Edwards. Polyol Complexes and Structure of the Benzeneboronate Ion - Google Scholar. *J. Org. Chem.*, 24(6):769–774, 1959.

[31] L. Luo, J. Jie, W. Zhang, Z. He, J. Wang, G. Yuan, W. Zhang, L. C. M. Wu, and S.-T. Lee. Silicon nanowire sensors for Hg2+ and Cd2+ ions. *Appl. Phys. Lett.*, 94(19):3101, 2009.

[32] M. H. Mashhadizadeh, I. S. Shoaei, and N. Monadi. A novel ion selective membrane potentiometric sensor for direct determination of Fe (III) in the presence of Fe (II). *Talanta*, 64(4):1048–1052, 2004.

[33] E. J. Menke, M. A. Thompson, C. Xiang, L. C. Yang, and R. M. Penner. Lithographically patterned nanowire electrodeposition. *Nat. Mater.*, 5(11):914–919, 2006.

[34] M. E. Meyerhoff and Y. M. Fraticelli. Ion-selective electrodes. *Anal. Chem.*, 54(5):27R—-44R, 1982.

[35] K. Mohan, K. C. Donavan, J. A. Arter, R. M. Penner, and G. A. Weiss. Sub-nanomolar detection of prostate-specific membrane antigen in synthetic urine by synergistic, dual-ligand phage. *J. Am. Chem. Soc.*, 135(20):7761–7767, 2013.

[36] B. Pappin, M. J. Kiefel, and T. A. Houston. Boron-Carbohydrate Interactions. In Chuan-Fa Chang, editor, *Carbohydrates - Compr. Stud. Glycobiol. Glycotechnol.*, chapter 3, pages 37–54. InTech, nov 2012.

[37] S. Park, H. Boo, and T. D. Chung. Electrochemical non-enzymatic glucose sensors. *Anal. Chim. Acta*, 556:46–57, 2006.

[38] R. M. Penner. Chemical sensing with nanowires. *Annual Review of Analytical Chemistry*, 5:461–485, 2012.

[39] R. M. Penner and G. A. Weiss. The promise of phage display: customized affinity and specificity. *Anal. Chem.*, 80(9):3082–3089, 2008.

[40] M. J. Pooyamanesh, H. A. Zamani, G. Rajabzadeh, M. R. Ganjali, and P. Norouzi. Fe (III) ion-selective membrane electrode based on 4-Amino-6-methyl-3-methylmercapto-1, 2, 4-triazin-5-one. *Anal. Lett.*, 40(8):1596–1609, 2007.

[41] M. Pourbaix. Atlas of electrochemical equilibria in aqueous solutions. 1974.

[42] M. M. Rahman, A. J. S. Ahammad, J.-H. Jin, S. J. Ahn, and J.-J. Lee. A Comprehensive Review of Glucose Biosensors Based on Nanostructured Metal-Oxides. *Sensors*, 10(5):4855–4886, may 2010.

[43] X. Ren and P. G. Pickup. Coupling of ion and electron transport during impedance measurements on a conducting polymer with similar ionic and electronic conductivities. *J. Chem. Soc., Faraday Trans.*, 89(2):321–326, 1993.

[44] H. J. Schugar, C. Walling, R. B. Jones, and H. B. Gray. The structure of iron (III) in aqueous solution. *J. Am. Chem. Soc.*, 89(15):3712–3720, 1967.

[45] K. Schügerl, B. Hitzmann, H. Jurgens, and T. Kullick. Challenges in integrating biosensors and FIA for on-line monitoring and control. *Trends Biotechnol.*, 14(1):21–31, 1996.

[46] P. Shen and Y. Xia. Synthesis-Modification Integration: One-Step Fabrication of Boronic Acid Functionalized Carbon Dots for Fluorescent Blood Sugar Sensing. *Anal. Chem.*, 86(11):5323–5329, jun 2014.

[47] D. J. Shirale, M. A. Bangar, W. Chen, N. V. Myung, and A. Mulchandani. Effect of aspect ratio (length: diameter) on a single polypyrrole nanowire FET device. *J. Phys. Chem. C*, 114(31):13375–13380, 2010.

[48] K.-K. Shiu, S.-K. Pang, and H.-K. Cheung. Electroanalysis of metal species at polypyrrole-modified electrodes. *J. Electroanal. Chem.*, 367(1):115–122, 1994.

[49] R. L. Solsky. Ion-selective electrodes. *Anal. Chem.*, 62(12):21R—-33R, 1990.

[50] H. G. Sudibya, Q. He, H. Zhang, and P. Chen. Electrical detection of metal ions using field-effect transistors based on micropatterned reduced graphene oxide films. *ACS Nano*, 5(3):1990–1994, 2011.

[51] D. K. Taggart, Y. Yang, S.-C. Kung, T. M. McIntire, and R. M. Penner. Enhanced thermoelectric metrics in ultra-long electrodeposited PEDOT nanowires. *Nano Lett.*, 11(1):125–131, 2010.

[52] K. Tanaka, T. Shichiri, S. Wang, and T. Yamabe. A study of the electropolymerization of thiophene. *Synth. Met.*, 24(3):203–215, may 1988.

[53] © International Diabetes Federation. *IDF DIABETES ATLAS*. International Diabetes Federation, seventh edition, 2015.

[54] S. J. Updike and G. P. Hicks. The Enzyme Electrode. *Nature*, 214(5092):986–988, jun 1967.

[55] S. Vaddiraju, D. J. Burgess, I. Tomazos, F. C. Jain, and F. Papadimitrakopoulos. Technologies for continuous glucose monitoring: current problems and future promises. *J. Diabetes Sci. Technol.*, 4(6):1540–62, nov 2010.

[56] A. K. Wanekaya, M. A. Bangar, M. Yun, W. Chen, N. V. Myung, and A. Mulchandani. Field-effect transistors based on single nanowires of conducting polymers. *J. Phys. Chem. C*, 111(13):5218–5221, 2007.

[57] T.-Y. Wang and J.-S. Shih. Iron (III) Ion Selective Electrode Based on Dithia 12-Crown-4. *J. Chinese Chem. Soc.*, 35(6):405–410, 1988.

[58] X. Wu, Z. Li, X.-X. Chen, J. S. Fossey, T. D. James, and Y.-B. Jiang. Selective sensing of saccharides using simple boronic acids and their aggregates. *Chem. Soc. Rev.*, 42(20):8032, 2013.

[59] C. Xiang, S.-C. Kung, D. K. Taggart, F. Yang, M. A. Thompson, A. G. Guell, Y. Yang, and R. M. Penner. Lithographically patterned nanowire electrodeposition: A method for patterning electrically continuous metal nanowires on dielectrics. *ACS Nano*, 2(9):1939–1949, 2008.

[60] C. Xiang, Y. Yang, and R. M. Penner. Cheating the diffraction limit: electrodeposited nanowires patterned by photolithography. *Chem. Commun.*, (8):859–873, 2009.

[61] L.-m. C. Yang, J. J. E. Diaz, T. M. McIntire, G. a. Weiss, and R. M. Penner. Direct Electrical Transduction of Antibody Binding to a Covalent Virus Layer Using Electrochemical Impedance - SUPPLIMENTARY MATERIAL. *Anal. Chem.*, 2(15):9–10, 2008.

[62] P. J. Yoo, K. T. Nam, J. Qi, S.-K. Lee, J. Park, A. M. Belcher, and P. T. Hammond. Spontaneous assembly of viruses on multilayered polymer surfaces. *Nat. Mater.*, 5(3):234–240, 2006.

[63] J. Zhang, W. Hodge, C. Hutnick, and X. Wang. Noninvasive diagnostic devices for diabetes through measuring tear glucose. *J. Diabetes Sci. Technol.*, 5(1):166–72, jan 2011.